

European Summer Wet-Bulb Temperature: Spatiotemporal Variations and Potential Drivers

QIYUN MA^a, YUMENG CHEN^b, AND MONICA IONITA^{a,c}

^a Alfred Wegner Institute Helmholtz Center for Polar and Marine Research, Bremerhaven, Germany

^b Department of Meteorology and NCEO, University of Reading, Reading, United Kingdom

^c Faculty of Forestry, “Stefan cel Mare” University of Suceava, Suceava, Romania

(Manuscript received 13 July 2023, in final form 29 December 2023, accepted 9 January 2024)

ABSTRACT: Heat stress is projected to intensify with global warming, causing significant socioeconomic impacts and threatening human health. Wet-bulb temperature (WBT), which combines temperature and humidity effects, is a useful indicator for assessing regional and global heat stress variability and trends. However, the variations of European WBT and their underlying mechanisms remain unclear. Using observations and reanalysis datasets, we demonstrate a remarkable warming of summer WBT during the period 1958–2021 over Europe. Specifically, the European summer WBT has increased by over 1.0°C in the past 64 years. We find that the increase in European summer WBT is driven by both near-surface warming temperatures and increasing atmospheric moisture content. We identify four dominant modes of European summer WBT variability and investigate their linkage with the large-scale atmospheric circulation and sea surface temperature anomalies. The first two leading modes of the European WBT variability exhibit prominent interdecadal to long-term variations, mainly driven by a circumglobal wave train and concurrent sea surface temperature variations. The last two leading modes of European WBT variability mainly show interannual variations, indicating a direct and rapid response to large-scale atmospheric dynamics and nearby sea surface temperature variations. Further analysis shows the role of global warming and changes in midlatitude circulations in the variations of summer WBT. Our findings can enhance the understanding of plausible drivers of heat stress in Europe and provide valuable insights for regional decision-makers and climate adaptation planning.

SIGNIFICANCE STATEMENT: Wet-bulb temperature, which takes into account the combined effect of temperature and humidity, is a good indicator for assessing heat stress. In the context of global warming, heat stress is anticipated to escalate, posing significant risks to human health and causing socioeconomic losses. However, variations in wet-bulb temperature and the associated physical mechanisms have received limited attention. This study aims to improve our understanding of the temporal and spatial variations and the potential driving mechanisms of summer wet-bulb temperature across Europe in recent decades. We have observed a noteworthy increase in summer wet-bulb temperature, indicating a regional intensification of heat stress, particularly within the last 10 years. We further investigate the connections between variations in summer wet-bulb temperature, large-scale atmospheric circulation, and sea surface temperature. Additionally, we explore their associations with global warming and changes in midlatitude atmospheric circulation. The outcomes of this study not only contribute to establishing a scientific basis for evaluating heat-related risks in Europe but also facilitate preparedness for future climate adaptation and mitigation at both regional and local scales.


KEYWORDS: Atmosphere; Europe; Atmospheric circulation; Climate change; Interannual variability; Interdecadal variability

1. Introduction

In recent decades, there has been a significant increase in the frequency, duration, and intensity of extreme heatwaves, particularly in the midlatitude regions (Russo et al. 2014; Horton et al. 2016; Ma and Franzke 2021). Moreover, climate models project a further intensification of these extreme heat events due to the ongoing anthropogenic global warming (Russo et al. 2014; Fischer and Knutti 2013; Coffel et al. 2018). Given their frequently disastrous social and economic consequences, these events have attracted growing scientific and

societal attention (Horton et al. 2016; Barriopedro et al. 2023). Multiple lines of evidence indicate that deadly heat events are not solely attributed to high temperatures but are also exacerbated by the effects of high humidity (Russo et al. 2017; Yu et al. 2021; Davis et al. 2016; Bekris et al. 2023). In hot environments, humidity levels play a crucial role in human thermoregulation (Raymond et al. 2020; Russo et al. 2017), as high humidity tends to impede the efficiency of human sweat-based latent cooling (Lin and Yuan 2022). Consequently, various heat stress indices, which consider the combined effects of temperature and humidity, have been proposed to quantify the impact of hot and humid conditions on human health (Stull 2011; Sherwood and Huber 2010; Matthews et al. 2022).

Wet-bulb temperature (WBT), as one of the heat stress indices, is a common and effective measure for assessing the impact of extreme heat waves on human health (Wang et al. 2019; Rogers et al. 2021). Previous research has considered the

 Denotes content that is immediately available upon publication as open access.

Corresponding author: Qiyun Ma, qiyun.ma@awi.de

DOI: 10.1175/JCLI-D-23-0420.1

© 2024 American Meteorological Society. This published article is licensed under the terms of a Creative Commons Attribution 4.0 International (CC BY 4.0) License



theoretical human physiological tolerance limit for WBT to be 35°C (Sherwood and Huber 2010; Buzan and Huber 2020). As a consequence, prolonged exposure to WBT above 35°C can lead to heat-related mortality and illnesses (Rogers et al. 2021). Under global warming, Raymond et al. (2020) reported that this theoretical threshold will be exceeded in some coastal subtropical locations. The observed increase in WBT and intensified heat stress are projected to persist across the globe (Li et al. 2017; Raymond et al. 2020; Wang et al. 2021; Coffel et al. 2018; Buzan and Huber 2020; Bekris et al. 2023). Therefore, investigating the mechanisms behind WBT variations is of great importance for regional climate prediction, risk assessments in heat stress, and for policymakers aiming to enhance adaptation to climate change.

Europe is experiencing accelerated warming compared to other land regions in the northern midlatitudes, primarily due to the significant influence of anthropogenic activities (Li et al. 2017). During the summer season, numerous extreme heat events have occurred over Europe in recent years, including the infamous 2003 European heatwave (Cassou et al. 2005), the 2010 Russian heat waves (Russo et al. 2014), and the record-breaking 2022 European heatwave (Rousi et al. 2022). These extreme heat events have had severe impacts on European ecosystems, agricultural yields, and have resulted in significant human and economic losses (Diffenbaugh et al. 2007; Ionita et al. 2022; Yu et al. 2021). However, when evaluated using WBT, lower WBT values around 28°C have been observed during these extreme heat events (Coffel et al. 2018). Stated by previous studies (Raymond et al. 2020; Rogers et al. 2021; Bekris et al. 2023), dangerous heat-induced mortality and morbidity impacts can occur at much lower WBT values, for example, around 27°C. This discrepancy in WBT values suggests variations in temperature measurements and heat stress calculations, as the latter considers the influence of humidity. Concerning the rates of increase in temperature and heat stress, earlier research suggests that the increase in temperature exhibits a larger magnitude of change compared to heat stress, which takes into account both temperature and moisture effects (Matthews et al. 2022; Rogers et al. 2021). The remaining unknown question is the relative contribution of surface temperature and humidity to the increase in European summer heat stress. Hence, gaining a better understanding of summer WBT and its underlying dynamics is paramount to predict and assess the risk of heat stress in Europe.

Considering temperature alone, significant progress has been made in the physical understanding of European summer heat waves (Ionita et al. 2013, 2020; Rousi et al. 2022; Barriopedro et al. 2023). A consensus is that the large-scale atmospheric circulation plays the most direct role compared to ocean circulation and overall global warming. This is primarily attributed to its association with persistent subtropical ridges and/or blocking anticyclones, which are essential factors in the development of heat waves (Ma and Franzke 2021; Barriopedro et al. 2023). Heat waves in midlatitude regions can be considered as regional manifestations of quasi-stationary Rossby waves (Barriopedro et al. 2023), which constitute a predominant part of the midlatitude circulation in the Northern Hemisphere (NH) (Coumou et al. 2015; Kornhuber et al. 2019). The changes in extratropical Rossby waves are largely forced by local and remote sea surface

temperature (SST) anomalies (Ma and Franzke 2021; Teng et al. 2022), while also being influenced by atmospheric internal variability (Coumou et al. 2018; Li et al. 2020). Moreover, soil moisture deficit and related land-atmosphere feedbacks (Fischer et al. 2007; Tuel and Eltahir 2021) play an important role in intensifying land surface hot temperatures. Furthermore, anthropogenically induced warming has also contributed to the occurrence of extreme hot summers in Europe, primarily due to the increase in greenhouse gas concentrations (Li et al. 2017; Raymond et al. 2020) and the reduction in emissions of anthropogenic aerosol precursors (Dong et al. 2017). Other influential factors have also been reported, such as changes in summer atmospheric circulations (Horton et al. 2015) and Arctic warming (Coumou et al. 2015).

However, little advance has been made in understanding the behavior and dynamics of WBT variability (Raymond et al. 2017; Rogers et al. 2021; Ning et al. 2022). In particular, there seems to be a lack of knowledge and research on WBT in Europe. Given the accelerated pace of warming over this region, there is an urgent need to quantify the variations and elucidate the driving mechanisms of European summer WBT in order to address the more serious heat-induced impacts. Several studies have focused on detecting the spatiotemporal patterns and investigating the anthropogenic influence of summer WBT variations at a global scale (Coffel et al. 2018), hemispheric scale (Li et al. 2017), and regional scale (Yu et al. 2021), as well as exploring the relative contributions of moisture and temperature to extreme WBT events (Raymond et al. 2017; Wang et al. 2019). As for exploring the driving mechanisms, Ning et al. (2022) analyzed the dominant modes and their dynamic mechanisms of summer WBT anomalies in China from 1960 to 2017, while the role of SST anomalies has not been clearly examined. Lin and Yuan (2022) investigated the relationships between different zonal wavenumbers embedded in amplified quasi-stationary waves and summer WBT extremes in the midlatitudes NH.

Here, we study the robustness of the spatial and temporal variations of summer WBT over Europe from 1958 to 2021 using both observation-based and reanalysis datasets. We investigate the dominant modes of summer WBT anomalies and explore the underlying large-scale driving mechanisms at multiple time scales, relying on both internal modes of variability and SST anomalies. Furthermore, we examine the potential linkages between variations in WBT anomalies and global warming as well as atmospheric circulation changes. Our overarching goal is to enhance our understanding of the warming of summer WBT over Europe, enabling better preparedness for and adaptation to global warming.

2. Data and methods

a. Data

Our analysis focuses on the European region, spanning from 36° to 70°N and 10°W to 45°E. We utilize both observations and reanalysis products to compute the WBT using 2-m air temperature, specific humidity, and relative humidity data. The primary dataset used is the Japanese 55-year Reanalysis (JRA-55; Kobayashi et al. 2015), which has a spatial resolution of 1.25° × 1.25° and a

temporal resolution of 6 h per day. To ensure the robustness of our findings, we incorporate high-resolution observations from the European Climate Assessment and Dataset (E-OBS, version v25.0e) provided by the European Climate Assessment and Dataset (Comes et al. 2018). E-OBS collects daily averaged observations from meteorological stations across Europe and provides a daily gridded dataset with a regular horizontal resolution of $0.1^\circ \times 0.1^\circ$. We compute the observational WBT by averaging 100 ensemble members of daily temperature and relative humidity from E-OBS (Ionita et al. 2021). To enable comparison with JRA-55, the computed WBT using E-OBS data is interpolated to the same spatial resolution as JRA-55. The analyzed datasets cover the period from 1958 to 2021.

To diagnose large-scale atmospheric and SST conditions influencing the variability of WBT, other variables from the JRA-55 dataset are also employed, including monthly geopotential height, meridional wind, zonal wind, and specific humidity. We also utilize the monthly Extended Reconstructed Sea Surface Temperature (ERSSTv5; Huang et al. 2017) dataset, which has a global spatial resolution of $2.0^\circ \times 2.0^\circ$.

Furthermore, we explore the relationships between the dominant modes of WBT and various large-scale internal modes of variability at multiple time scales, ranging from interannual to multidecadal scales. The climate indices used in this study include the monthly Atlantic multidecadal variability (AMV), the Arctic Oscillation (AO), the North Atlantic Oscillation (NAO), the El Niño–Southern Oscillation index (Niño-3.4), and the Indian Ocean Dipole Mode Index (DMI). All these indices are directly sourced from the KNMI (the Royal Netherlands Meteorological Institute) Climate Explorer. In this study, we specifically examine the contemporaneous associations between major climate modes and European WBT variations during the boreal summer. Future investigations should consider the influence of large-scale climate modes from the prior winter or spring on summer WBT variations (e.g., Martija-Díez et al. 2021).

b. Calculation of wet-bulb temperature

Various methods have been developed to quantify heat stress [see Table 1 in Buzan et al. (2015) and references therein]. Among these methods, WBT has emerged as a commonly used index for assessing human-perceived heat stress in recent research (Raymond et al. 2020; Wang et al. 2019). However, it is important to note that the calculation of WBT can vary across studies (Ning et al. 2022; Rogers et al. 2021; Knutson and Ploshay 2016), depending on data availability and computational resources. In this study, we employ two different methods to estimate WBT, thus facilitating the evaluation and strengthening the reliability of our results.

Our calculation of WBT primarily relies on the Davies-Jones method (WBT_{DJ}), as proposed by Davies-Jones (2008) and implemented by Buzan et al. (2015). Previous studies have found that this method is particularly accurate at high temperatures, making it widely applicable in research on WBT extremes (Coffel et al. 2018; Raymond et al. 2020), even though it is more complex and computationally intensive compared to empirical

formulas (Rogers et al. 2021). A detailed description of the computation process can be found in Buzan et al. (2015).

For a more direct comparison between E-OBS and JRA-55, we also compute WBT_S using a simplified algorithm developed by Stull (2011). This algorithm estimates WBT (°C) at standard sea level pressure as follows:

$$\begin{aligned} \text{WBT}_S = & T \times \arctan[0.151\,977 \times (\text{RH} + 8.313\,659)^{0.5}] \\ & + \arctan(T + \text{RH}) - \arctan(\text{RH} - 1.676\,331) \\ & + 0.003\,918\,38 \times (\text{RH})^{1.5} \\ & \times \arctan(0.023\,101 \times \text{RH}) - 4.686\,035 \end{aligned} \quad (1)$$

where T represent the 2-m air temperature (°C) and RH is the relative humidity (%). This formula is easy to implement and provides an indication of the evaporative cooling efficiency of the human body (Zhao et al. 2021). It has been found to be accurate within specific ranges of relative humidity (5%–99%) and air temperature (20°–50°C), which are relevant for our summertime analysis. The WBT_S has also been widely used in various regions and climate conditions, including studies by Raymond et al. (2017) for the contiguous United States and Ning et al. (2022) for mainland China.

We first calculate both WBT_{DJ} and WBT_S at 6-h intervals per day using the JRA-55 dataset. Subsequently, we average these values to obtain daily averaged WBT. Seasonal means are then computed from the daily averaged data. To calculate anomalies for WBT and other variables, we subtract the climatological mean over the period of 1981–2010 in this study.

To justify the appropriate utilization of the JRA-55 dataset, we first conduct a comparative assessment of the results obtained using the two methods for calculating WBT. Our focus is on their variations and long-term trends during the summer season. Subsequently, due to data availability, we compute WBT_S using the E-OBS dataset and compare these values with the WBT_S derived from the JRA-55 dataset. It is worth noting that some missing values exist over eastern and south-eastern Europe in the E-OBS dataset, so our comparisons are limited to the grid points where values are available in both datasets.

c. Estimate of trend and significance test

Two methods are used to quantify the summer WBT trend. First, we estimate the long-term linear trend using least squares linear regression over the entire European region. Second, we detect the spatially nonlinear monotonic trend at each grid point using the Mann–Kendall (MK) method, a nonparametric statistical test widely used for detecting long-term trends in hydroclimatic time series (Ionita et al. 2021; Ma et al. 2021). To account for the presence of serial correlation within the time series and mitigate spurious trends, we employ the trend-free prewhitening technique proposed by Yue and Wang (2002). The magnitude of the trend is then evaluated using the nonparametric Sen's slope estimator.

For assessing the statistical significance of the identified trends, we consider a trend to be significant only if it is significant at the 5% level. To address the challenge of multiple hypothesis testing,

we apply a false discovery rate (FDR) correction following the approach suggested by Wilks (2016). This correction provides a rigorous assessment of trend significance by adjusting the p values obtained from the MK test. We control the FDR by setting the FDR-adjusted significance level (α_{FDR}) to 0.1. This implies that we expect 10% of the identified significant grid points to fulfill the null hypothesis, although this test may be conservative for spatially correlated data (Wilks 2016; Lin and Yuan 2022).

d. Identification of dominant modes and its large-scale drivers

To identify dominant modes of variability in summer WBT anomalies, we employ empirical orthogonal function (EOF) analysis. This analysis effectively separates modes with distinct spatial patterns and their corresponding temporal principal components (PCs). Prior to the analysis, we remove the global warming trend by linearly detrending the WBT anomalies using a least squares regression fit. We also apply a weighting scheme based on the square root of the cosine of the latitude. The significance of the detected modes is evaluated using North's rule of thumb (North et al. 1982), which determines the sampling error of each mode to ensure nondegenerate EOFs.

Regression and correlation analyses are conducted to explore the relationships between large-scale internal modes of variability, atmospheric variables, and the identified PCs for each mode at various time scales. To capture the interdecadal to multidecadal component, locally weighted scatterplot smoothing (LOWESS; Cleveland 1979) is utilized for different PCs and internal modes of variability. LOWESS is advantageous in considering nonlinearities in the data, as opposed to a simple linear regression (Rousi et al. 2022). A LOWESS with a 17% span, approximately 11 years, is applied here for this purpose.

Composite analysis is used to investigate the atmospheric circulations and SST anomalies associated with each dominant EOF mode. Geopotential height and wind anomalies at 500 hPa are computed to represent the corresponding atmospheric circulations, and similar analysis is performed for SST anomalies. To gain insight into the physical mechanisms associated with each EOF mode, composite maps are constructed based on the PC time series for years when PC values exceed (high composite) or fall below (low composite) one standard deviation (Ionita et al. 2013, 2020). The differences between the high and low composite maps are calculated. For composite maps, the statistical significance is assessed using a Student's t test at a 5% significance level.

Additionally, we examine the connection between summer WBT variations and changes in midlatitude circulations from the perspective of atmospheric eddy kinetic energy (EKE). Following Coumou et al. (2015), we focus on the changes of synoptic transients over the midlatitudes, which are associated with synoptic-scale high and low pressure systems. EKE serves as a measure of the interplay between the intensity and frequency of these involved high and low pressure systems (Coumou et al. 2015; Lehmann et al. 2014). Previous studies have documented a weakening of summertime EKE in the NH, which is associated with an increased occurrence of extreme heat events during boreal summer (Coumou et al. 2015).

To calculate EKE, we apply a 2.5–6-day bandpass filter to daily wind fields, focusing on synoptic-scale (eddy) activity (Lehmann and Coumou 2015). The calculation is as follows:

$$\text{EKE} = 0.5 \times (u'^2 + v'^2), \quad (2)$$

where u' and v' represent the zonal and meridional wind speeds after bandpass filtering, respectively. We compute the EKE at 500 and 850 hPa to ensure the robustness of our analysis. The summertime EKE is obtained by averaging the daily EKE values. EKE is calculated for the period from 1979 to 2021 using JRA-55 data, taking into account the potential effects of changes in the observing system starting from the modern satellite era (1979 onward) for calculating atmospheric energy (Ma et al. 2021) and the reported period of weakening summer circulation in the NH (Coumou et al. 2015).

Quantile regression (Koenker and Bassett 1978) is then employed to examine the relationship between EKE and WBT variations. Unlike linear regression, quantile regression estimates the effects of changes not only in the mean, but also in all parts of the EKE distribution, ranging from the 10th to 90th percentiles (Hirschi et al. 2011). This method does not rely on assumptions about the parametric form of the underlying probability distribution (Rhines et al. 2017), making it suitable for analyzing trends and changes in percentile values of climate variables (Gao and Franzke 2017). Recently, this method has been utilized to establish a link between summer heat extremes and reduced storm track activity across large midlatitude continental regions (Lehmann and Coumou 2015).

3. Climatology, validation, and trend analysis of summer WBT

The climatological pattern of summer mean WBT exhibits a south high–north low feature (Figs. 1a,b). The coastal region around the Mediterranean and the north of the Black Sea show higher WBT values around 20°C, while lower values (around 10°C) are generally observed over the Fennoscandian Peninsula and high-elevation regions like the Alps. This geographical pattern of summer WBT could be closely attributed to the warmer and drier Mediterranean climate in southern Europe and the colder and more humid subarctic climate in northern Europe (Peel et al. 2007). Notably, this climatological pattern remains consistent regardless of the method used for WBT calculation (Figs. 1a,b). Previous studies suggest the importance of method choice when considering humid extreme events (Rogers et al. 2021), we therefore compare the spatial distribution of differences obtained using two WBT calculation methods (Fig. 1c). We analyze their differences by subtracting the results from the WBT_DJ from the results obtained using the empirical Eq. (1). The differences do not exceed 0.9°C. In comparison, WBT_S tends to slightly underestimate (overestimate) WBT values in the northern (southeastern) parts of Europe compared to WBT_DJ. For central Europe, both methods yield nearly identical results. Moreover, statistically significant positive correlations were found between the seasonal variations in WBT estimated from WBT_DJ and WBT_S, with correlation values exceeding 0.95 for almost all the grid cells (not shown). The results suggest that both methods

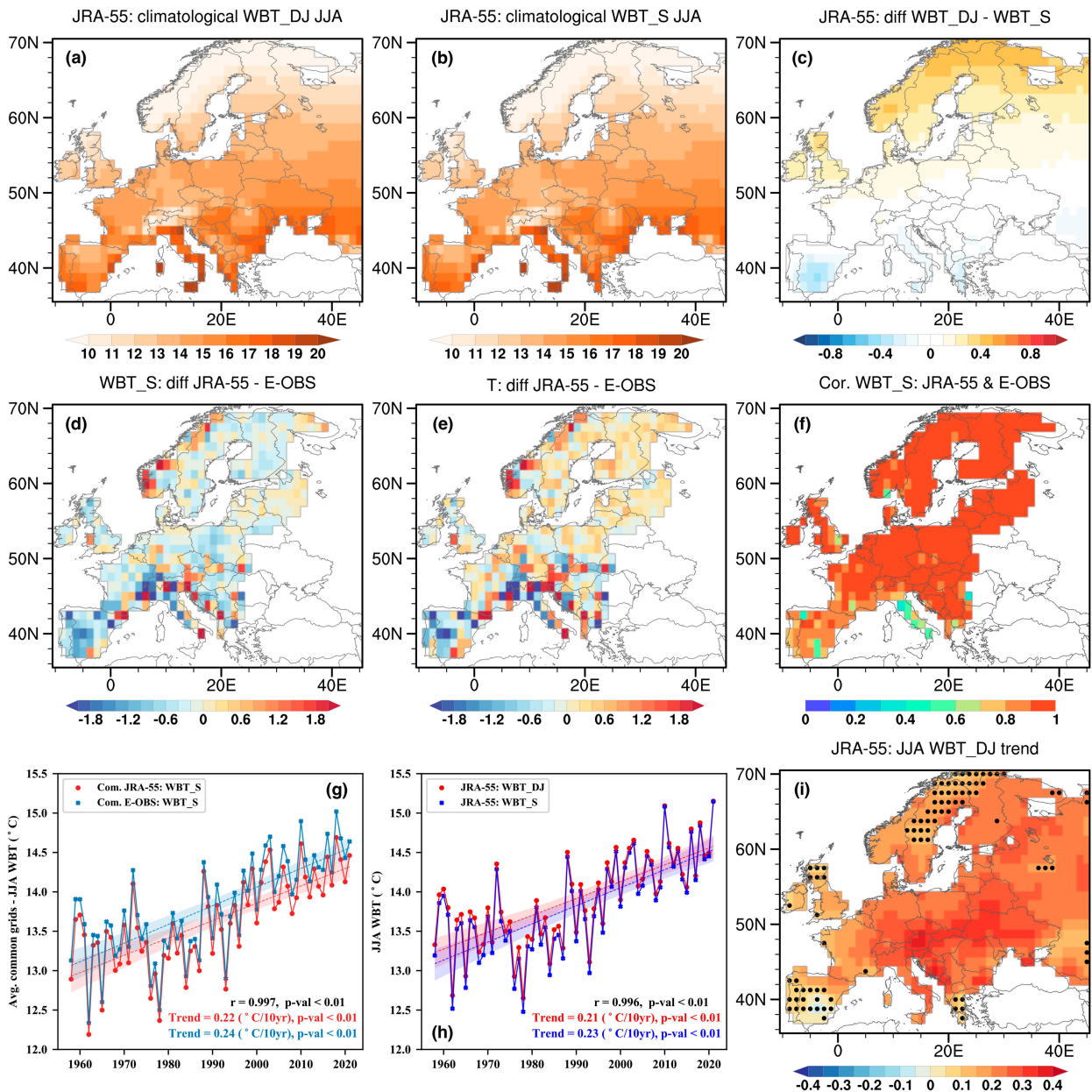


FIG. 1. Climatological patterns ($^{\circ}\text{C}$) and trends ($^{\circ}\text{C decade}^{-1}$) of European summer mean WBT from 1958 to 2021. Climatological patterns obtained from JRA-55: (a) WBT_DJ, (b) WBT_S, and (c) their difference. The difference between (d) WBT_S and (e) surface temperature between JRA-55 and E-OBS over their common grid cells. (f) The correlation of the estimated WBT_S between the two datasets. (g) Comparison of the two datasets in the time series and linear trends for the European averaged summer WBT_S over the common grid cells. (h) As in (g), but showing the European averaged summer WBT_DJ and WBT_S using JRA-55. Shading in (g) and (h) indicates 90% confidence intervals for the estimated slope. (i) Trend of European summer WBT_DJ using JRA-55. Stippling indicates where the trends are *not* statistically significant according to the FDR test.

are reasonable and consistent for estimating European summer WBT variations using the JRA-55 dataset.

We then estimate WBT_S using high-resolution observational E-OBS data to validate the results from JRA-55 data. The E-OBS data displays many grid points with missing values in eastern Europe, primarily due to the quality control check process, especially for relative humidity observations

(Cornes et al. 2018). Therefore, we compare the two datasets by considering the common grid cells, meaning that both datasets have WBT_S values estimated. As shown in Fig. 1d, compared with E-OBS, JRA-55 appears to exhibit general warm biases in the estimated WBT_S over eastern Europe and the Fennoscandian Peninsula, while displaying cold biases over southern and western Europe. These warm and cold

biases in WBT_S are primarily caused by the surface temperature bias of JRA-55 (Fig. 1e). Relative humidity is expected to play a minor role in the estimated bias of WBT_S for the two datasets, as it contributes less to the variations in summer WBT_S compared to surface temperature (shown in Fig. 2a, the black dotted line), aligning with global-scale findings reported by Knutson and Ploshay (2016). While biases are evident in the estimated WBT_S in JRA-55 over Europe, significant positive correlations are observed between the two datasets, particularly in central and northern Europe (Fig. 1f). The correlations over southern Europe are smaller, although still significant. We note that these lower correlations are mainly due to the relatively larger surface temperature bias in estimating WBT_S in JRA-55 (Fig. 1e), resulting in a different magnitude of the increasing rate in WBT_S compared to E-OBS, as observed over Italy (not shown). We further analyze the temporal evolution and linear trend of European summer WBT_S, averaging it over the common grid cells for both datasets presented in Fig. 1g. We observe a general cold bias in JRA-55, with an increasing trend of $0.22^{\circ}\text{C decade}^{-1}$, slightly smaller than that in E-OBS ($0.24^{\circ}\text{C decade}^{-1}$). The significant positive correlation is evident, with a value of 0.997 ($p < 0.01$). These findings support the rational use of JRA-55 for studying variations in European summer WBT.

Regarding both temporal variations and the linear trend, the disparities between WBT_DJ and WBT_S, as calculated from the JRA-55 dataset, are minimal (Fig. 1h), corroborating the outcomes presented in Figs. 1a–c. The time series of European regional average WBT_DJ and WBT_S demonstrate a significantly strong positive correlation ($r = 0.996$, $p < 0.01$) and display nearly identical increasing trends from 1958 to 2021. The linear warming trend for WBT_DJ ($0.21^{\circ}\text{C decade}^{-1}$) is marginally less than the corresponding trend estimated for WBT_S ($0.23^{\circ}\text{C decade}^{-1}$). The regional average summer WBT_DJ values are slightly higher than those of WBT_S in most years. This observation corroborates the findings of previous research by Buzan et al. (2015), which showed that WBT_DJ is more effective in capturing high WBT values. Therefore, WBT_DJ will be employed to represent European summer WBT variations throughout the remainder of this study. In subsequent analyses, unless otherwise specified, WBT will denote WBT_DJ for brevity.

A detailed examination of the temporal variations in summer WBT reveals a significant period of rapid warming over Europe that began in the late 1980s (Fig. 1h). This warming trend aligns with the signal of anthropogenic climate change (Li et al. 2017). Since the 1980s, Europe has experienced a noteworthy reduction in anthropogenic aerosols, primarily attributable to stringent air quality regulations (Smith et al. 2011). This decline in aerosols has been linked to the rapid warming observed over Europe, as it results in increased downward solar radiation and positive local land–atmosphere feedbacks (Dong et al. 2017). In the meantime, other drivers have also become more evident, such as the phase shifting of the low-frequency variations of SST in the Atlantic Ocean (Sutton and Hodson 2005), changes in midlatitude circulations (Horton et al. 2016), and the rapid and substantial decline in Arctic sea ice (Vihma 2014).

In terms of spatial distribution, the majority of the European region has experienced a significant increase in summer WBT, while there are limited areas showing insignificant increasing trends (Fig. 1i). These less affected regions include the southern Iberian Peninsula, the northern British Isles, and the northeastern Scandinavian Peninsula. In contrast, the more pronounced increases in WBT are primarily concentrated in central and southern Europe, characterized by trends ranging from 0.2° to $0.4^{\circ}\text{C decade}^{-1}$, which indicates a regional amplification of heat stress. In conclusion, central Europe, characterized by the highest population density (Buzan and Huber 2020), warrants heightened vigilance due to the steadily increasing risk of summer heat stress in these regions.

4. Contributors and distribution of the increasing summer WBT

a. Contributions of temperature and humidity

To understand the increasing trends in European summer WBT, we investigate the relative impacts of temperature and humidity changes, as these are critical components in WBT estimation (Raymond et al. 2017; Bekris et al. 2023). In doing so, we carry out a sensitivity analysis to reevaluate summer WBT, considering constant specific humidity or constant surface temperature. The constant values are calculated using their long-term mean values spanning from 1958 to 2021. When assuming constant specific humidity, the regional increase in WBT is primarily driven by surface temperature alone, and vice versa. As shown in Fig. 2a, increases in surface temperature contribute substantially to the warming of summer WBT, accounting for an average of 57% of the increase in WBT (Fig. 1h), while specific humidity accounts for the remaining 43%. This suggests that both temperature and humidity changes contribute to the increasing summer heat stress in Europe, with temperature effects slightly more dominant than changes in the specific humidity. This conclusion is further supported when examining the linear trends of temperature and specific humidity individually, where the increasing trend of temperature ($0.31^{\circ}\text{C decade}^{-1}$) is slightly larger than that of other variables. Our findings align with the global-scale results reported by Knutson and Ploshay (2016). Additionally, it is interesting to note that the trend of WBT with constant temperature differs between WBT_S (slightly decreasing) and WBT_DJ (increasing). This result further supports the preference for using WBT_DJ, emphasizing the potential misinterpretations that could arise from using WBT_S to assess regional WBT variations.

The re-evaluated spatial trends of European summer WBT are depicted in Figs. 2b and 2c. When assuming constant specific humidity, the spatial pattern closely resembles that obtained using concurrent specific humidity in Fig. 1i, with generally lower trends in central and southern Europe. Notable differences emerge over the Fennoscandian Peninsula, revealing an increasing trend that is not statistically significant, and over the Iberian Peninsula, transitioning from a nonsignificant decreasing trend to a significant increasing trend. This identified spatial pattern aligns similarly with the trends in surface temperature alone (Fig. 2d), although the magnitudes are slightly smaller. In contrast, assuming constant

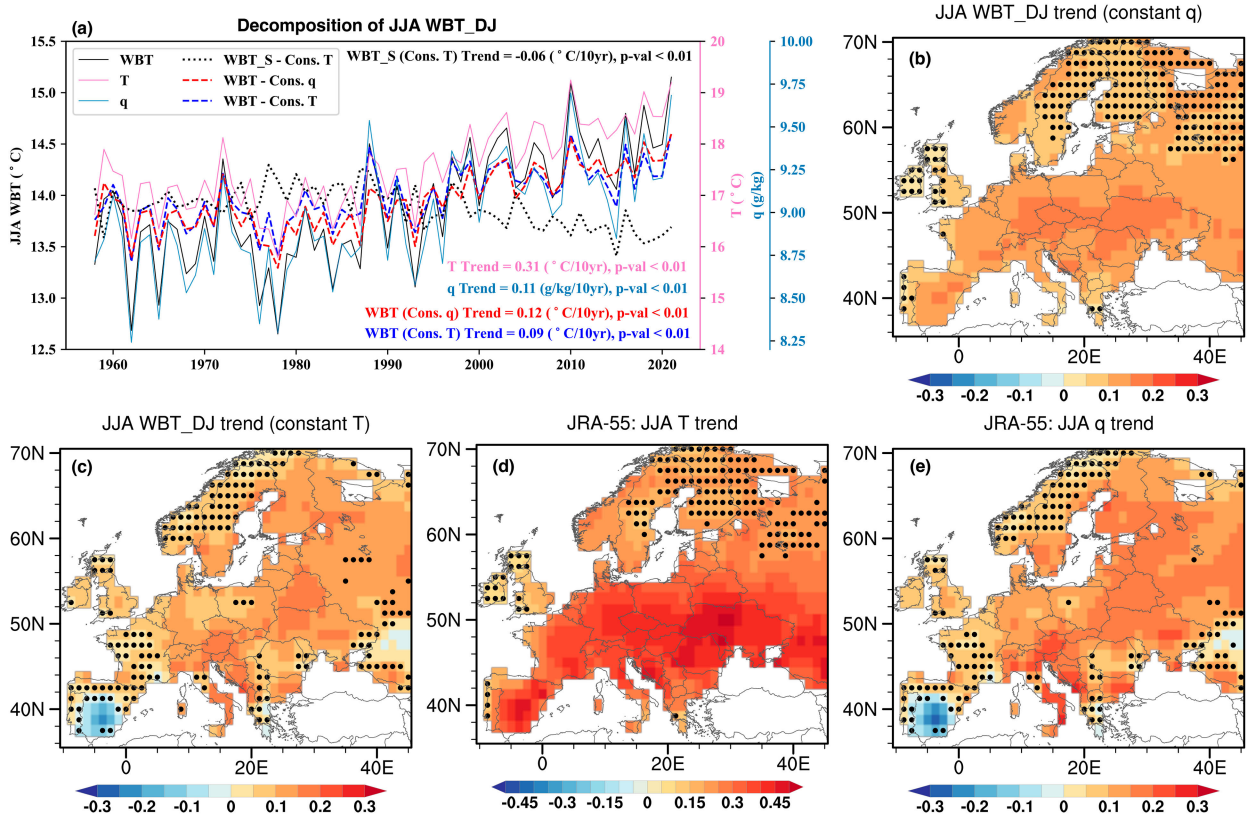


FIG. 2. Contributions of temperature and humidity to European summer WBT variations. (a) Time series and linear trends of European summer mean surface temperature (T ; $^{\circ}\text{C}$), specific humidity (q ; g kg^{-1}), WBT_S assuming constant surface temperature, WBT_DJ assuming constant specific humidity, and surface temperature, respectively. Unless otherwise stated, hereafter WBT is used to represent WBT_DJ in short. (b)–(e) Spatial distribution of linear trends of the variables shown in (a); units are $^{\circ}\text{C decade}^{-1}$, except for (e), which is in $\text{g kg}^{-1} \text{ decade}^{-1}$. Stippling indicates where the trends are *not* statistically significant according to the FDR test.

surface temperature also yields a comparable pattern to Fig. 1i, with significant increasing trends mainly scattered in the southern and northeastern regions. However, a significant decreasing trend in summer WBT is observed over most parts of the Iberian Peninsula. This decline is attributed to a significant decrease in specific humidity, leading to a reduction in air moisture content in this region (Fig. 2e), as a result of the inherently dry climate and declining summer precipitation in recent decades (Liu et al. 2022). It is noteworthy that the significant rise in regional surface temperature (Fig. 2d) suggests that dry heatwaves may become more severe and more frequent, owing to an intensified land–atmosphere interaction over the Iberian Peninsula (Tuel and Eltahir 2021; Fischer et al. 2007). In summary, our findings suggest that the increase in European summer WBT is attributed to both rising summer temperatures and a simultaneous increase in air moisture content, as indicated by the rise in specific humidity (Byrne and O’Gorman 2018; Brogli et al. 2019).

b. Changes in summer WBT variability

We analyze changes in the probability density distributions (PDFs) of summer WBT from a statistical perspective. We consider three time periods: 1958–89, 1990–2021, and 2012–21. Here, the summer WBT values for the three periods are

calculated by removing the mean value from the reference period (1981–2010). The spatial distribution of summer mean WBT values is then presented in Figs. 3a–c, respectively. The warm values of summer WBT are becoming more pronounced across nearly all regions from 1990 to 2021, aligning with the trend pattern in Fig. 1i. Notably, significant warming has occurred in the last decade (2012–21), with central Europe experiencing an increase of over 1°C and the high-latitude region around the Fennoscandian Peninsula witnessing an approximate 0.5°C rise. These warming patterns are generally consistent with the findings of Yu et al. (2021) and Li et al. (2017). This motivates us to further assess the changing distributions of summer WBT over Europe.

Figure 3d presents the estimated PDFs and related statistics for the three periods, along with the PDF for the reference period used for comparison. To evaluate significant differences compared to the reference period, we employ two statistical tests: the two-sample Kolmogorov–Smirnov test and the Student’s t test, using a significance level of 0.05. All three PDFs pass both of these statistical tests, indicating statistically significant changes. When comparing the periods of 1958–89 and 1990–2021, we observe a significant increase in the mean WBT of 0.73°C . This shift in the entire PDF toward the

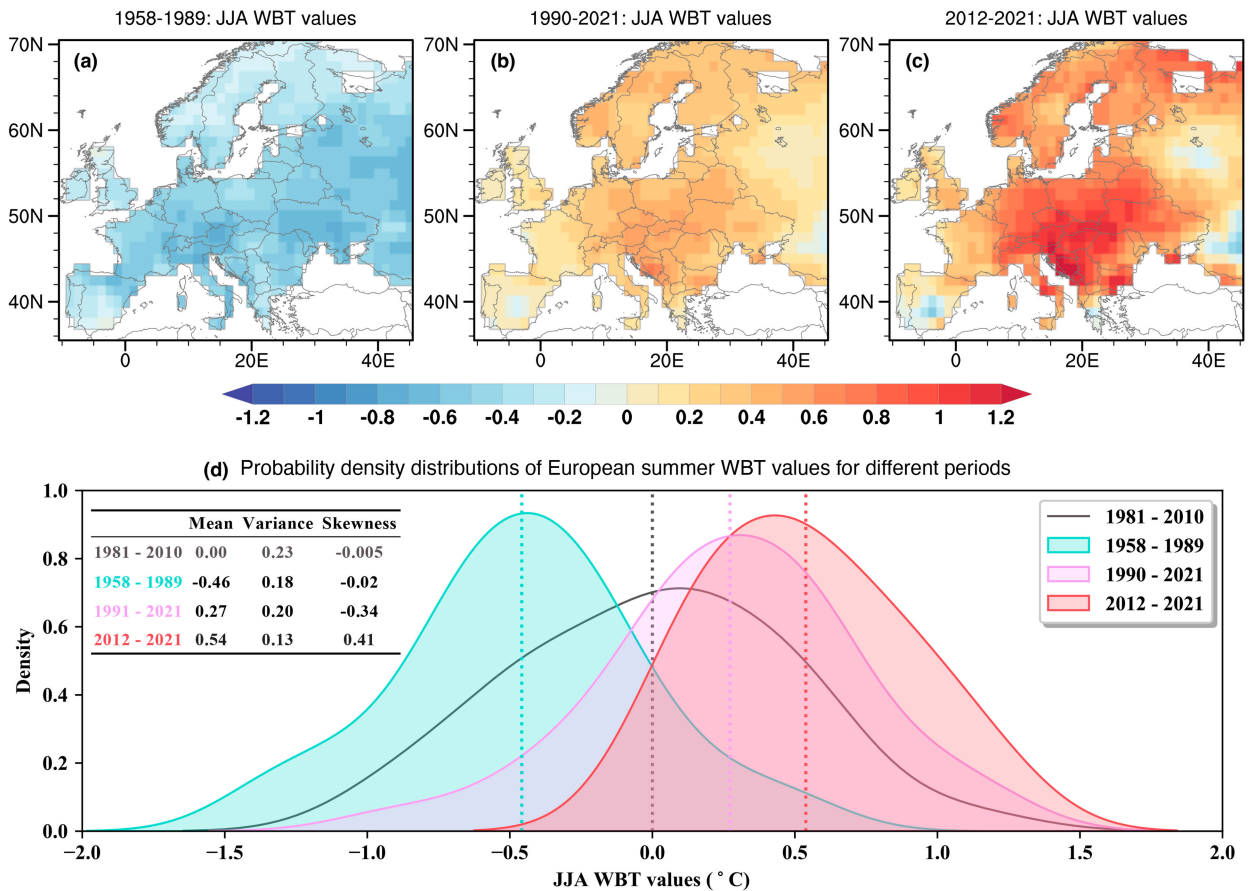


FIG. 3. Spatial distribution of summer WBT values ($^{\circ}\text{C}$) for the periods (a) 1958–89, (b) 1990–2021, and (c) 2012–21. Summer WBT values are determined by removing the mean value from the reference period (1981–2010). (d) Changes in probability density functions (PDFs) of European regionally averaged summer WBT values during the three periods, along with statistics for shape, scale, and location parameters. The dashed vertical lines represent the mean values of each distribution. The grayed line represents the PDF for the reference period. All the other PDFs pass the significance test when compared with the referenced PDF.

warmer part of the distribution results in a more negatively skewed distribution, while the variance remains largely unchanged. However, in the comparison of the periods 1958–89 and 2012–21, we not only observe a shifted mean but also discern alterations in symmetry, as indicated by changes in both the mean and skewness (Kodra and Ganguly 2014). Our findings reveal that summer mean WBT has warmed by 1.0°C over the past decade. Given the significant impacts of anthropogenic global warming (Li et al. 2017), the risk of heat stress is expected to increase, posing a substantial threat to human health in the coming decades.

5. Dominant modes of summer WBT anomalies

To understand the influences of large-scale climate variability, we conduct the EOF analysis to unveil the dominant modes of variability in summer WBT anomalies over the period 1958–2021. We employ data from a total of 64 summer seasons for this EOF analysis. The first four leading EOF modes and their corresponding PC time series are selected and depicted in Figs. 4 and 5. These modes have all passed the statistical significance

test (North et al. 1982), indicating their distinctiveness from one another and their clear separation from any remaining higher modes. It is worth noting that we performed the same procedure using summer monthly anomalies of WBT and E-OBS data separately, which resulted in consistent spatial patterns for the first four leading EOF modes (not shown). This consistency reinforces our confidence in the robustness and reproducibility of these four EOF modes for characterizing European summer WBT variations.

In total, the four primary seasonal EOF modes identified collectively explain approximately 81% of the total variance, highlighting their capability to capture the spatiotemporal characteristics of European summer WBT anomalies. It is important to note that the spatial patterns of the EOFs are represented as the regression of the detrended summer WBT anomalies onto the corresponding PCs. To better illustrate the overall warming pattern over Europe, the PCs are inverted by multiplying them by -1 . As shown in Fig. 4, the first two EOF modes reflect generally the natural low-frequency variations in summer WBT anomalies. EOF1 represents a homogeneous monopolar warming pattern over central to eastern Europe (Fig. 4a). The corresponding PC1

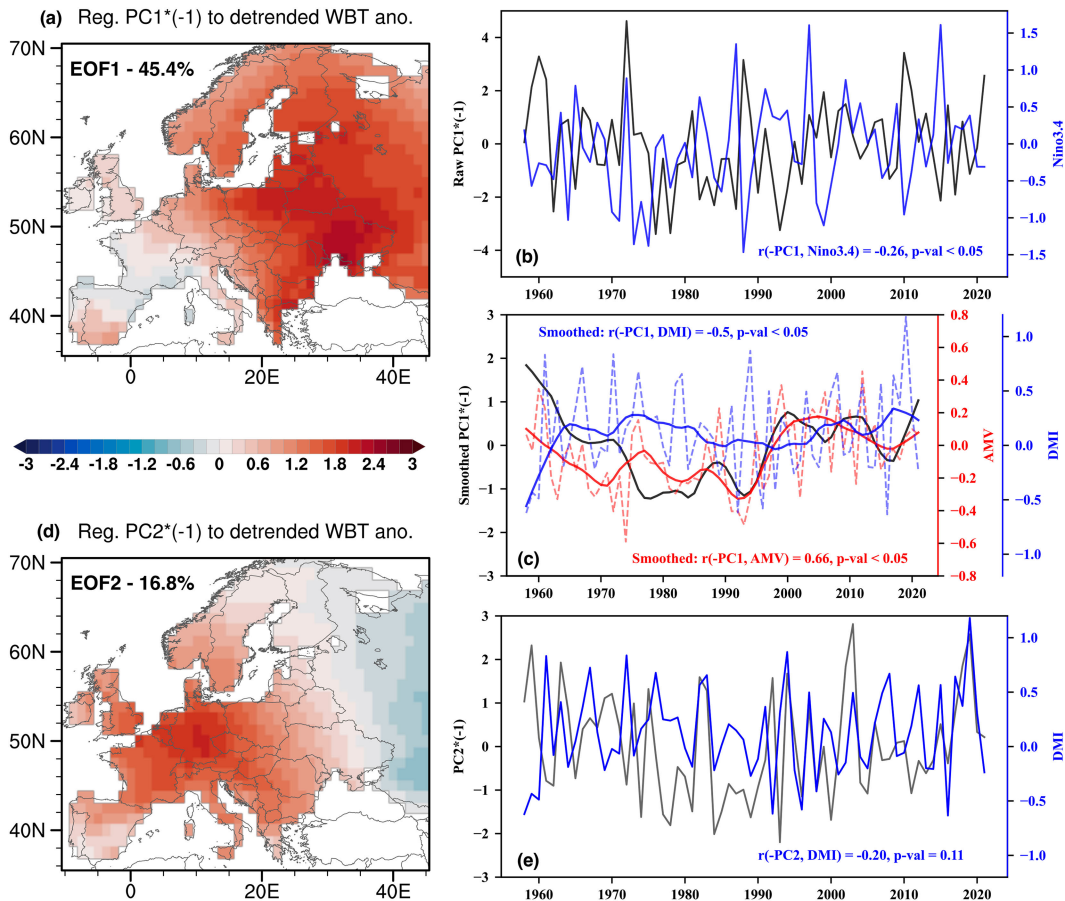


FIG. 4. The spatial patterns for the (a) first (EOF1) and (d) second (EOF2) EOF modes. The percent of the total variance explained by each EOF is shown in the top left. Also shown are the corresponding standardized principal components (PCs) for (b),(c) EOF1 and (e) EOF2, along with their statistically significant correlated climate indices. The PCs are normalized based on their standard deviations. The dashed lines show the smoothed LOWESS curve fit with a span of 0.17. The spatial patterns of EOFs ($^{\circ}\text{C}$) are expressed as the regression of the detrended summer WBT anomalies against PCs.

exhibits pronounced interdecadal (Fig. 4b) to multidecadal (Fig. 4c) variations, indicating regional transitions from warm to cold and then back to warm climate periods. This mode may be linked to the AMV, which plays a significant role in the multidecadal variations of European summer temperature (Sutton and Hodson 2005; Ghosh et al. 2017). Regarding EOF2, it displays a zonal-like dipole pattern (Fig. 4c), with warm anomalies in the western-to-southwest part of Europe and cooling in the eastern part of Europe. This spatial pattern could be associated with SST anomalies over the Indian Ocean and western Pacific (Behera et al. 2013). The PC2 primarily exhibits intradecadal to interdecadal variations (Fig. 4e), with a shift toward a warmer regime in summer WBT anomalies since the mid-1990s, particularly over western Europe. This aligns with the recent warming trends shown in Fig. 3c and with observations reported by Dong et al. (2017).

In contrast, the high-frequency variations of summer WBT anomalies are mainly captured by EOF3 and EOF4. EOF3 shows a meridional-like dipole pattern (Fig. 5a), characterized by negative anomalies over the northwestern part of Europe and

positive anomalies over much of the southern region. The PC3 tends to capture interannual to intradecadal variability (Fig. 5b). The spatial pattern of EOF3 resembles the temperature pattern influenced by the summer NAO in Europe (Folland et al. 2009; Li et al. 2020), suggesting potential impacts of the variations in the NAO. Concerning EOF4, it displays a tripole-like pattern (Fig. 5c), with negative anomalies over southwestern and northeastern Europe, and positive anomalies stretching across central Europe from the Scandinavian Peninsula to regions around the Black Sea and the Caspian Sea. As shown in Fig. 5d, the PC4 reflects mainly the interannual variability of summer WBT anomalies.

6. Possible drivers of the dominant modes

a. Contributing factors

Before delving into the role of atmospheric circulation in WBT variability, we first briefly examine the influence of temperature, humidity, and moisture fluxes on the four dominant modes. To achieve this, we perform a regression analysis using detrended

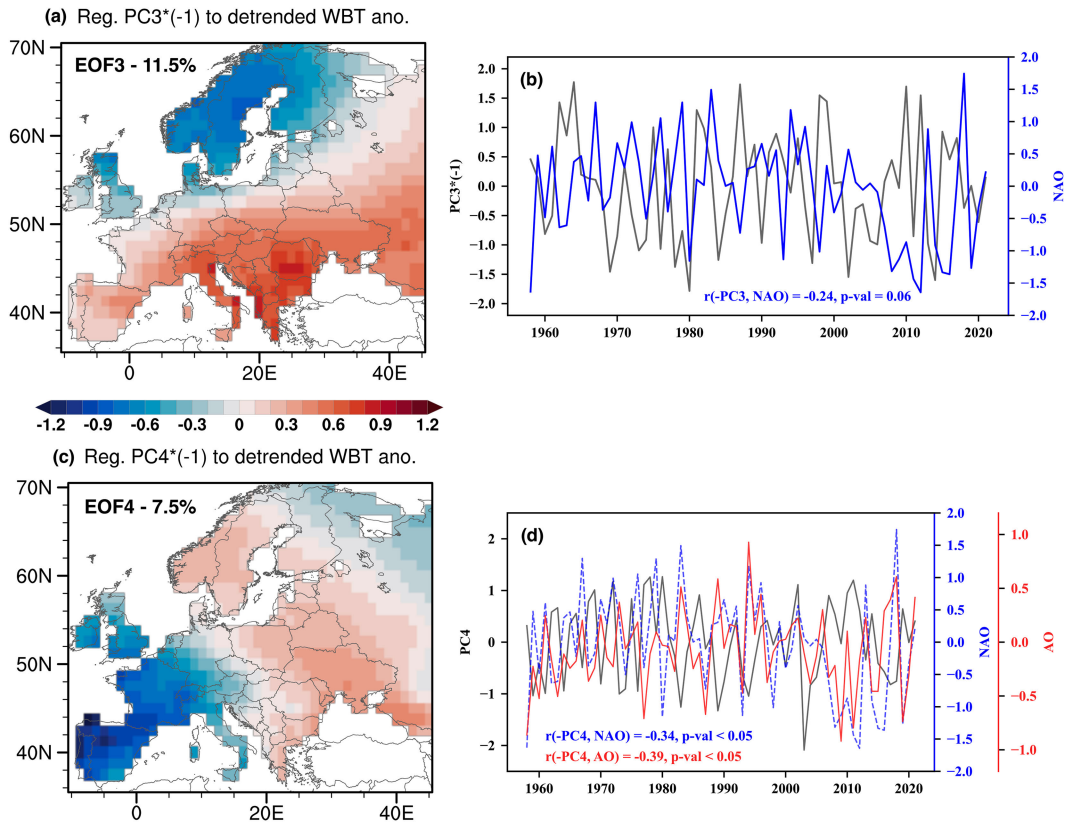


FIG. 5. As in Fig. 4, but for the third and fourth EOF modes.

anomalies of temperature, specific humidity, and moisture variables in relation to the leading mode PCs. We note that the temperature and specific humidity data used in the regression analysis have been detrended from the original data, without assuming a constant variable as in the previous section. Additionally, we explore the low-level moisture transport and moisture convergence at 850 hPa associated with these modes.

For all four modes, the significant anomaly patterns of temperature (Figs. 6a,d,g,j) and specific humidity (Figs. 6b,e,h,k) exhibit a coherent phase with the corresponding spatial patterns of each EOF mode. These findings confirm the concurrent influence of temperature and humidity on European summer WBT variations, with temperature playing a more substantial role, particularly in the first two EOF modes. The interannual variations are primarily linked to temperature changes over southern Europe (cf. Figs. 6g,j with Figs. 6h,k). Regarding the contributions of moisture flux and its associated divergence (Figs. 6c,f,i,l), the centers of moisture divergence generally coincide with the regions of anomalous warm temperatures, indicating that water vapor tends to diverge from those locations. In contrast, cooling anomalies are typically associated with the convergence of moisture fluxes, such as over the Fennoscandian Peninsula in Fig. 6i. In summary, temperature and specific humidity make positive contributions to the spatial patterns of the dominant EOF modes, while moisture fluxes tend to play a contrasting role that is positively correlated with water vapor convergence. This complex interplay of temperature, humidity,

and moisture fluxes contributes to the variability of summer European WBT.

b. Composites of large-scale atmospheric circulation anomalies

To elucidate the potential mechanisms behind the dominant modes, we examine the corresponding atmospheric circulation anomalies using summertime geopotential height and wind anomalies at 500 hPa. We present the composite maps for both the high and low composites, as well as their differences. For PC1, the high composite map exhibits widespread positive geopotential height anomalies across eastern Europe and small areas of negative anomalies centered around the British Isles (Fig. 7a). Conversely, the low composite shows pronounced negative anomalies spreading over Europe (Fig. 7b). The centers of the anomalies align well for the two composites. The differences between the high and low composites (Fig. 7c) reveal deepened positive (negative) circulation anomalies centered over eastern Europe (the British Isles). The high composite of PC1, as shown in Fig. 4a, has been influential in Europe since the mid-1990s (Fig. 4b), indicating the dominance of circulation anomalies similar to those in Fig. 7a in the current climate. Previous studies suggest that high pressure anomalies over the North Atlantic can be associated with the advection of warm air from the tropical ocean (Cassou et al. 2005), while another positive center over eastern Europe can directly warm that region by enhancing incoming solar radiation and reducing

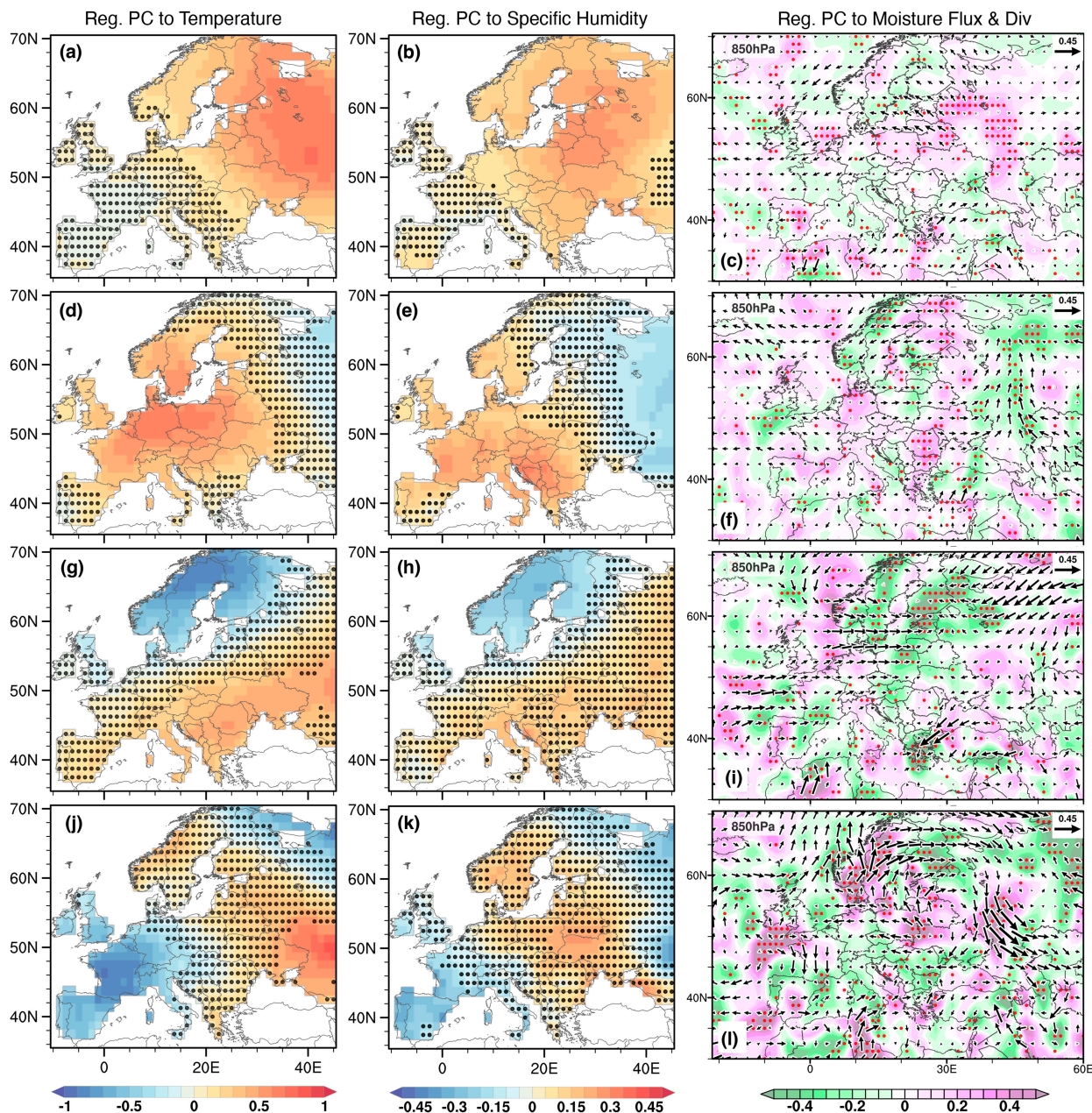


FIG. 6. Regression maps of air temperature, specific humidity, and moisture flux convergence [shading: $\text{g} (\text{m}^2 \text{s}^{-1})$] and moisture transport at 850 hPa (vectors; $\text{g kg}^{-1} \text{m s}^{-1}$) onto the standardized series of (a)–(c) PC1, (d)–(f) PC2, (g)–(i) PC3, and (j)–(l) PC4. The black (red) stippling indicates where areas are *not* (are) statistically significant at the 95% level by the Student's *t* test. The moisture fluxes are shown after using a nine-point smoothing method for improved visualization.

cloud cover (Ma and Franzke 2021). Furthermore, as suggested by Fig. 6c, heat and moisture from other remote regions, such as the eastern Mediterranean, may also contribute to sustaining the circulation anomalies, as discussed in Zschenderlein et al. (2019).

An omega-like blocking structure is identified, centered over central Europe, in both the high and low composite maps of PC2 (Figs. 7d,e). The blocking system is particularly prominent in the differences between the high and low composite

maps (Fig. 7f), which reveal two distinct anomalous low anomalies located over the subpolar gyre region in the North Atlantic and over northeast Europe extending toward the Arctic. The presence of this blocking circulation anomalies over Europe plays a crucial role in disrupting the westerly flow, allowing for the advection of warm air from the subtropical region, thereby further intensifying the high pressure anomalies (Teng et al. 2022; Zschenderlein et al. 2019). This, in turn, leads to a regional weather pattern characterized by warm and dry conditions. The

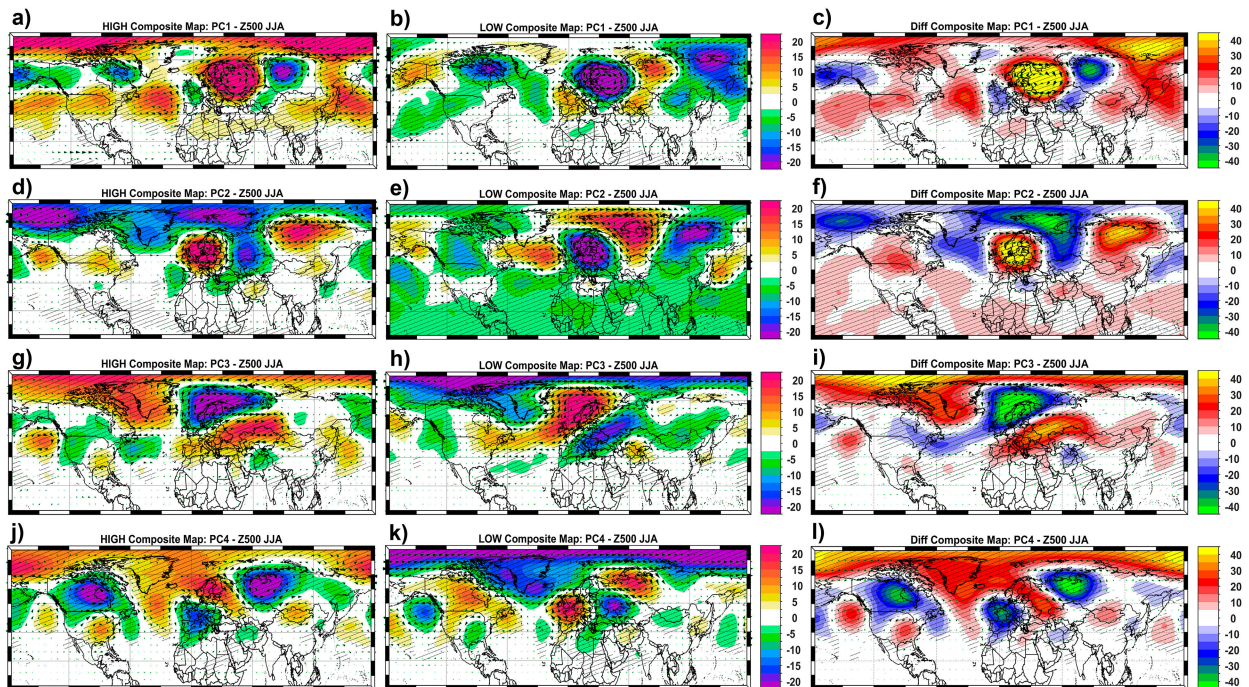


FIG. 7. Composite large-scale circulation anomalies for the four dominant modes of summer WBT anomalies. The high (low) composite includes the summer when the corresponding PC values are greater (lower) than one standard deviation. (a)–(c) High and low composite and their differences for EOF1. Composite of geopotential height (shading; m) and wind (vectors; m s^{-1}) anomalies at 500 hPa. Other panels are as in (a)–(c), but for (d)–(f) EOF2, (g)–(i) EOF3, and (j)–(l) EOF4. The hatched areas indicate anomalies that are statistically significant at the 95% significance level.

consistent anomaly centers between the high and low composites, particularly over land areas, suggest a well-characterized contribution of the North Atlantic variability to this mode. Additionally, as suggested by previous studies (Behera et al. 2013; Ma and Franzke 2021), SST anomalies from remote regions, such as the tropical Indian Ocean and Pacific Ocean, may play a crucial role in maintaining these blocking circulation anomalies over Europe. A more in-depth discussion of the role of SST anomalies will be presented in the next section.

When examining the entire NH, we observe a resemblance between the combined influence of the first two EOF modes and a circumglobal midlatitude wave train as proposed by Saeed et al. (2014). This wave train plays a critical role in affecting summer moisture convergence over Europe, distinct from the impacts of the summer NAO. To elucidate the relationships between this wave train and the first two PCs of European summer WBT variations, we construct a circumglobal midlatitude wave train index (CGTI) following the method of Saeed et al. (2014). The CGTI is defined as the principal component associated with the first EOF mode of summer 200-hPa meridional wind anomalies over the domain spanning from 20° to 80°N and from 100°W to 100°E . As shown in Fig. 8a, the time series of CGTI and the first two PCs present a strong linear relationship. The joint probability kernel density, presented in Figs. 8b and 8c, indicates evident linear relationships between CGTI and the two PCs, respectively. A significant correlation is identified between PC1 and CGTI ($r = 0.63$, $p < 0.01$), and a weaker correlation is also found for PC2

($r = 0.23$, $p = 0.06$). To highlight their associations with CGTI, a linear combination of the first two PCs ($-PC1 + PC2$) reveals a more substantial relationship with CGTI ($r = 0.69$, $p < 0.01$). Thus, our results suggest that the proposed circumglobal wave train exerts a dominant influence on the first two leading modes of European summer WBT anomalies. Additionally, these two leading modes capture variations in summer WBT at interdecadal to multidecadal time scales and could be linked to large-scale SST anomalies, such as the AMV (Ghosh et al. 2017).

Regarding PC3, the spatial structure of the composite maps (Figs. 7g–i) resembles the weather regime associated with different phases of summer NAO (Cassou et al. 2005; Ferranti et al. 2015) or a mixture of European blocking and Scandinavian blocking (Hochman et al. 2021). In the high composite, there are anomalously high (low) pressure conditions over southeastern (northwestern) Europe (Fig. 7g), which is inverted in the low composite (Fig. 7h). The difference between the high and low composite years exhibits a strengthened circulation anomalies similar to the high composite (Fig. 7i). These results are consistent with previous studies on the relationships between summer NAO variations and temperature anomalies (Bladé et al. 2012; Li et al. 2020). Furthermore, we find a significant correlation ($r = -0.24$, $p < 0.05$) between the summer NAO index and PC3 (Fig. 5b), confirming the influence of NAO in modulating summer WBT at the interannual time scale.

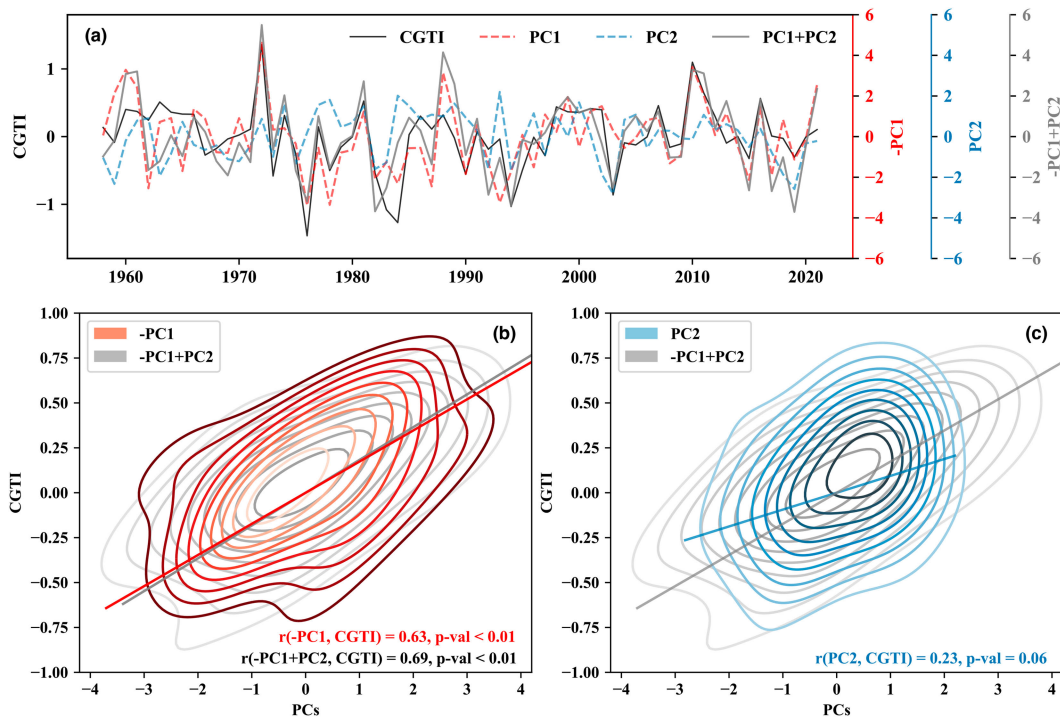


FIG. 8. The relationship between CGTI and the PCs of the first two leading EOFs of summer WBT anomalies. (a) Time series. (b) The joint probability density distribution of CGTI and PC1, as well as linear combinations of the first two PCs ($-PC1 + PC2$). (c) As in (b), but for the PC2.

The composite circulation anomalies for PC4 reveal a higher wavenumber pattern over the NH compared to the other modes, exhibiting a meridional-like tripole structure over Europe (Figs. 7j–l). In the high composite, two anomalous low pressure systems are observed over the Iberian Peninsula and around the Barents Sea (Fig. 7j), while a high pressure system extends from southwestern Greenland to southwestern Europe. However, in the low composite, the centers of these anomalies do not perfectly match (Fig. 7k). This meridional-like pattern could be related to the variability of summer storm tracks over the North Atlantic (Dong et al. 2013), which are influenced by the summer AO and NAO (Coumou et al. 2018; Thompson and Wallace 2001). We examined the significant correlations between PC4 and AO ($r = -0.39, p < 0.05$) and NAO ($r = -0.34, p < 0.05$), as shown in Fig. 5d. The presence of correlations with both modes is not surprising, given the similarities between AO and NAO, with NAO sometimes considered a regional manifestation of AO (Thompson and Wallace 1998; Cohen and Barlow 2005). Notably, the AO and NAO indices exhibit relatively larger variations after the late 1990s, potentially related to the recent intensification of Arctic amplification (Coumou et al. 2018), which warrants further investigation. Furthermore, the high wavenumber pattern and its connection to the circumglobal teleconnection over the NH may contribute to the variation of PC4 (Kornhuber et al. 2019), while further investigations are needed to fully understand its role. In short, our results suggest that NAO and AO are relevant climate modes influencing summer WBT variations at the interannual scale, potentially working together to induce variations of WBT over the Iberian Peninsula (Fig. 3).

c. Connection to the SST anomalies

As previously mentioned, variations in SST have significant impacts on European summer climate at multiple time scales. For instance, multidecadal variations in North Atlantic SST have been shown to influence European summer climate (Sutton and Hodson 2005; Sutton and Dong 2012; Ionita et al. 2015, 2017, 2022), as well as interannual SST variations in the tropical Indian Ocean and Pacific Ocean (Cassou et al. 2005; Behera et al. 2013; Ma and Franzke 2021). To examine the relationship between SST anomalies and the dominant modes of summer WBT anomalies, we conducted a composite analysis of SST anomalies (Fig. 9).

For PC1, the high (low) composite of PC1 exhibits significantly warm (cold) anomalies over the North Atlantic (Figs. 9a,b). The differences between the high and low composite maps (Fig. 9c) show a consistent pattern with the high composite map. Obvious SST anomalies are also observed in the Pacific and Southern Ocean. In the high composite, there is anomalous warming (cooling) over the eastern (western) Pacific, suggesting a relationship with ENSO. We find a significant correlation between PC1 and Niño-3.4 with a value of -0.26 ($p < 0.05$, Fig. 4b). Using the LOWESS method, we further highlight the impact of interdecadal to multidecadal SST variations on summer WBT, with a significant correlation of -0.5 ($p < 0.05$) for the DMI and 0.66 ($p < 0.05$) for the AMV (Fig. 4c). Our findings support previous research indicating that decadal to multidecadal variations in European summer climate are associated with SST variations over the North Atlantic (Sutton and Dong 2012; Ghosh et al. 2017; Della-Marta et al. 2007; Ionita et al. 2013). We demonstrate

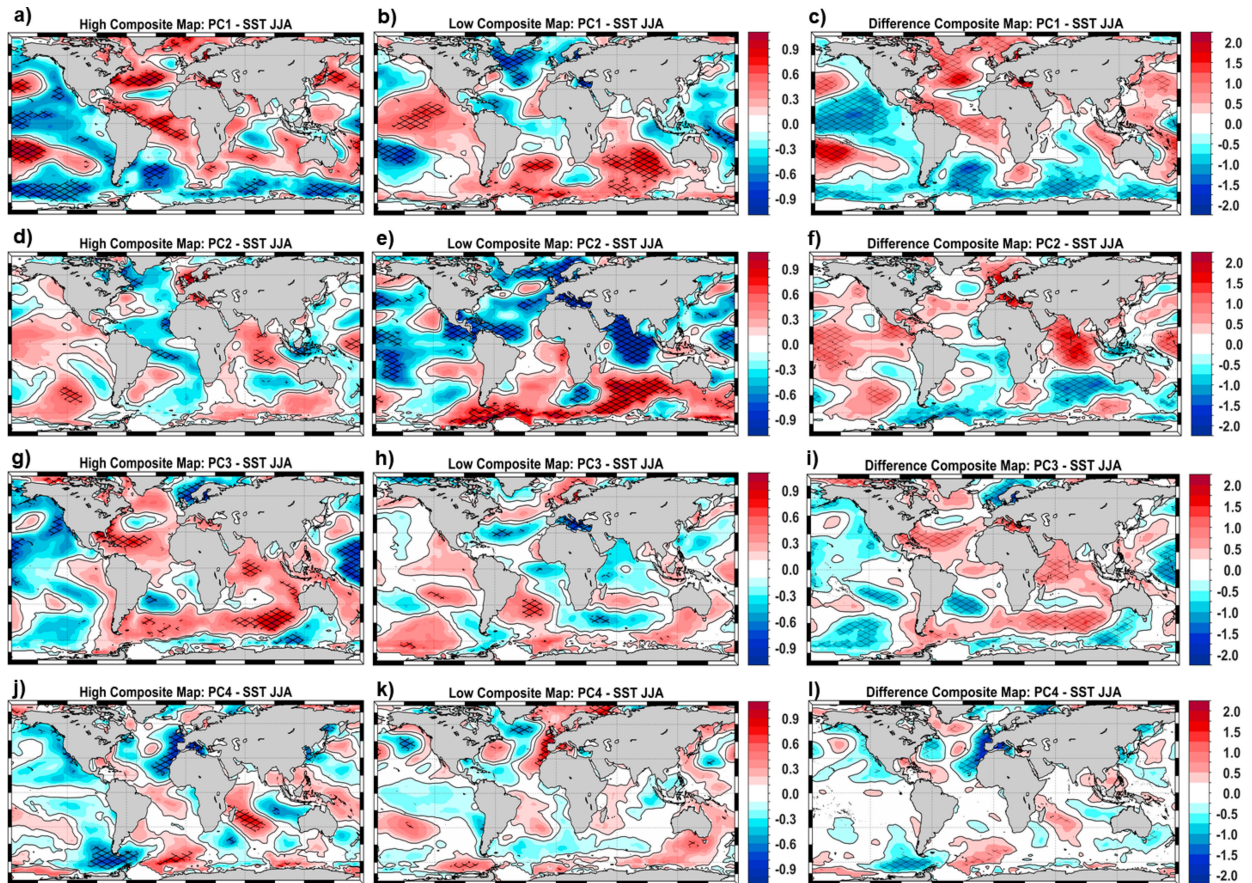


FIG. 9. As in Fig. 7, but for sea surface temperature anomalies.

that remote SST variations in the Indian and Pacific Oceans can also play a role in summer WBT variations.

For PC2, the SST anomalies exhibit strong anomalous SST mainly over the Mediterranean Sea and the Indian Ocean (Figs. 9d–f). The high composite and the differences between high and low composites show a more significant pattern. During the high composite phase, positive SST anomalies along the Mediterranean Sea could contribute to the warming of WBT through warm advection (Diffenbaugh et al. 2007). We also find a weak correlation between PC2 and the DMI ($r = -0.20$, $p = 0.11$), partly revealing the connections with SST anomalies over the Indian and western Pacific Oceans. This is supported by model experiments conducted by Ma and Franzke (2021), in which they demonstrate that anomalous heating over the western Indian and Pacific Ocean can trigger a wave train, influencing summer heatwaves over Europe. Therefore, we suggest that the accelerated warming of the tropical Indian Ocean (Hu and Fedorov 2019) may partly contribute to the current increase in summer WBT, although the pattern is not statistically significant in the composite analysis.

We also observe anomalous warming along the southeastern U.S. coast and the Gulf of Mexico in the patterns of PC1 (Fig. 9a), PC2 (Fig. 9e), and also PC3 (Fig. 9g). According to Saeed et al. (2014), the warming SST anomalies over these

regions can trigger the positive phase of the circumglobal mid-latitude wave train, which could influence the current European summer WBT, consistent with the circulation anomalies in the composite of PC1 (Fig. 7a) and PC2 (Fig. 7d). This provides additional evidence supporting the role of the circumglobal wave train in shaping European summer WBT variability. More in-depth dynamical analysis is encouraged for further explore this linkage.

Different from the first two PCs, the anomalous SST composites for PC3 (Figs. 9g–i) and PC4 (Figs. 9j–l) are primarily concentrated over the Mediterranean Sea or show SST variations over the North Atlantic region. In the composites for PC3, the anomalous SST patterns exhibit a distinct NAO pattern over the mid- and high-latitude North Atlantic, which is consistent with the circulation composites (Figs. 7g–i) and in agreement with previous studies (Folland et al. 2009). Regarding PC4, the SST anomalies are predominantly distributed along the coast of the Iberian Peninsula, northern Africa, and the western Mediterranean. These SST anomalies correspond well with the circulation anomalies over the ocean (Figs. 7j–l). Our findings suggest that there are rapid and interannual responses of WBT to SST anomalies at the same time scale, primarily through their fast influence on atmospheric circulations and/or warm-air advection.

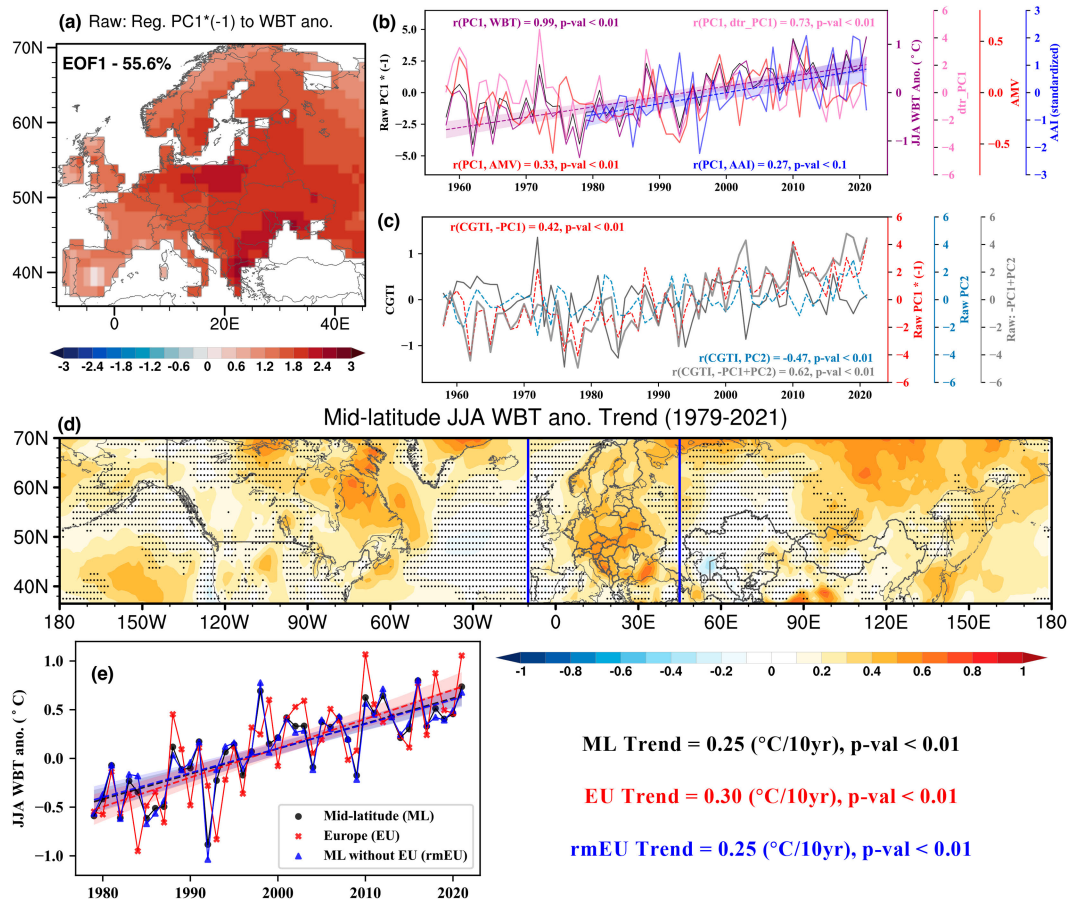


FIG. 10. (a) As in Fig. 4a, but for the EOF1 for the raw summer WBT anomalies ($^{\circ}\text{C}$). (b) Time series of non-detrended PC1 with its statistically significant correlated climate indices. (c) As in Fig. 8a, but for the nondetrended first two PCs. (d) As in Fig. 1d, but for trends in summer WBT anomalies ($^{\circ}\text{C decade}^{-1}$) for the period 1979–2021. (e) Time series of regionally averaged summer WBT anomalies of all land grid points: the midlatitudes (ML, 35° – 70°N), the defined European region (EU), and the midlatitudes excluding the EU (rmEU).

7. Linkage with global warming and midlatitude circulation changes

a. Global warming

So far, we have investigated the potential driving mechanisms behind the changes in summer WBT by considering the influence of large-scale climate variability. It is also important to examine how summer WBT responds to global warming. For this purpose, we conducted an EOF analysis using the nondetrended anomalies of summer WBT. The four EOF modes closely resemble those obtained from the detrended anomalies of summer WBT in Figs. 4 and 5. We focus on the first leading mode EOF1 (raw EOF1, Fig. 10a), as it explains a larger variance (55.6%) than the detrended EOF1 (45.4%; Fig. 4a). The raw EOF1 indicates a spatially increasing trend of summer WBT as shown in Fig. 1i. The corresponding PC1 exhibits a significant increasing trend (Fig. 10b) and has a strong correlation ($r = 0.99$, $p < 0.01$) with the raw, nondetrended time series of summer WBT anomalies. Additionally, a significant correlation ($r = 0.73$, $p < 0.01$) is also observed with the detrended PC1. These results

demonstrate that the raw EOF1 captures the trend in summer WBT associated with global warming and its internal decadal to multidecadal variations. Thus, the difference in explained variance is likely primarily due to the impact of anthropogenic-induced warming (Knutson and Ploshay 2016; Li et al. 2017), assuming a linear relationship between global warming and changes in summer WBT. Using observations and climate model outputs, Li et al. (2017) suggested that the total effect of anthropogenic forcing could contribute to approximately 1°C warming of summer WBT in the NH, with a particularly pronounced impact over Europe.

The influence by AMV is also clear, as evidenced by a significant correlation of 0.33 ($p < 0.01$). Even after applying the LOWESS filtering, the correlation value is 0.68, which remains almost equal with the detrended PC1 in Fig. 4c. This indicates that the role of the AMV in modulating summer WBT is not affected by the background warming. Previous studies have documented that SST over the North Atlantic has shifted to a phase characterized by anomalous warmth in the late 1990s (Sutton and Hodson 2005). This phase shift is associated with

northward ocean heat transport, leading to significant warming of the North Atlantic Ocean, as depicted in Fig. 9a. This warm anomaly over the North Atlantic contributes to anomalous warming over Europe through the prevailing westerly weather system. Additionally, previous studies have argued that the AMV is closely related to the Atlantic meridional overturning circulation (AMOC) (Dima and Lohmann 2007; DelSole et al. 2011). Recent observations and projections suggest that the AMOC is projected to transition to its negative phase in the future (Caesar et al. 2018; Latif et al. 2022). This transition is expected to result in a general cooling trend during European summers (Jackson et al. 2015). The cooling effect associated with the slowdown of the AMOC could partially mitigate the significant anthropogenic warming impact on Europe. However, the weakening of the AMOC remains a subject of debate (Jackson et al. 2015; Caesar et al. 2018; Latif et al. 2022). We recommend further research involving modeling and observations to gain a better understanding of the intricate interactions between the AMOC and global warming and how these interactions can impact European summer WBT.

The connection between the first two raw PCs and the circumglobal midlatitude wave train is evident as well, as depicted in Fig. 10c. Under the influence of global warming, the constructed CGTI exhibits significant correlations with both of these PCs. Specifically, the correlation is 0.42 ($p < 0.01$) for raw PC1 and -0.47 ($p < 0.01$) for PC2. Furthermore, the linear combination of the first two PCs reveals an even more significant correlation with CGTI ($r = 0.62$, $p < 0.01$). These results suggest that the wave train plays a robust and important role in modulating summer WBT at multiple time scales.

In recent decades, the Arctic has undergone significant climate warming with a rapid reduction in Arctic sea ice (Vihma 2014; Pedersen et al. 2016) and concurrent a noteworthy increase in near-surface temperatures (Screen and Simmonds 2010). This phenomenon, known as Arctic amplification, has been linked to substantial impacts on summer weather and climate in Europe (Francis and Vavrus 2012; Coumou et al. 2018; Zhang et al. 2020). To quantify Arctic amplification, we introduce the Arctic Amplification Index (AAI), defined as the temperature difference between the Arctic region (70° – 90° N) and midlatitudes (30° – 60° N) (Ionita et al. 2020) during the summer season. Data are analyzed from 1979 to 2021 due to observational uncertainties in earlier periods in high latitudes, primarily stemming from limited spatial coverage (England et al. 2021). As shown in Fig. 10b, the AAI demonstrates a significant increasing trend of approximately $0.16^{\circ}\text{C decade}^{-1}$ ($p < 0.01$), indicating intensified warming in the Arctic during the summer season. A weak correlation of 0.27 ($p < 0.1$) is observed between AAI and the nondetrended PC1. This finding is partly consistent with the research conducted by Zhang et al. (2020), who examined the influence of diminishing Arctic sea ice on decadal variations in European summer climate. These findings suggest a potential connection between recent Arctic amplification and the rising WBT in European summers, although its impacts on European climate are more pronounced during the winter season (Vihma 2014; Cohen et al. 2014).

Furthermore, we find that over the same period (1979–2021), the rate of increase in summer WBT over the European region is the highest among other land regions in the midlatitudes of the NH (Figs. 10d,e), which aligns with previous studies (Brogi

et al. 2019, 2021; Li et al. 2018). Specifically, European summer WBT exhibits an average increase of $0.30^{\circ}\text{C decade}^{-1}$, compared to $0.25^{\circ}\text{C decade}^{-1}$ for the rest of the midlatitudes. This rate of increase is slightly higher than the overall rate considering the entire time period ($0.21^{\circ}\text{C decade}^{-1}$) shown in Fig. 1i, indicating an acceleration in the warming trend over Europe in recent decades within the context of ongoing global warming.

b. Trends in midlatitude circulation

The increase in summer WBT can also be attributed to changes in atmospheric circulation. Previous studies have established a connection between the frequent occurrence of warm extremes and changes in atmospheric circulation over specific midlatitude regions (Barriopedro et al. 2023; Rousi et al. 2022). These changes in midlatitude circulation have been associated with Arctic amplification, which alters atmospheric dynamics by reducing the temperature gradient between the equator and the poles (Cohen et al. 2014; Coumou et al. 2018). As a result, summer circulation in the midlatitudes weakens (Coumou et al. 2015), leading to more meandering midlatitude jets and amplified stationary waves (Francis and Vavrus 2012), as well as an increased frequency of anticyclonic circulation systems during summer, including over Europe (Horton et al. 2015). Therefore, in our study, we examine the trends in midlatitude circulation changes by analyzing the variations in EKE.

During the period from 1979 to 2021, a consistent decline in summertime EKE has been observed in both the middle (500 hPa) and lower (850 hPa) troposphere (Figs. 11a,b). The most significant reduction in EKE is observed around southern Greenland and over central and eastern Europe, and this spatial pattern persists throughout the middle to lower troposphere. The decrease in EKE corresponds well with the increase in WBT over Europe (Fig. 10c), with a clearer relationship observed at the lower troposphere (Fig. 11b). This is consistent with findings from previous studies (Coumou et al. 2015; Ma et al. 2021), indicating a spatial weakening of atmospheric circulation. The weakened circulation is suggested to be associated with the occurrence of double jet flow regimes, as proposed by Rousi et al. (2022), which could prolong high-temperature events and consequently contribute to the warming of the summer mean climate over Europe. At the European level, the decline in summer EKE is also evident and robust at both pressure levels, particularly at 850 hPa, with a decline rate of $-0.14 \text{ m}^2 \text{ s}^{-2} \text{ decade}^{-1}$ (Fig. 11c). Significant negative correlations are identified between regional averaged summer WBT anomalies and EKE, with a value of -0.38 ($p < 0.05$) at 500 hPa and -0.50 ($p < 0.01$) at 850 hPa. The declining trend in EKE reflects an increase in positive geopotential height anomalies (Lehmann and Coumou 2015), which suggests a higher occurrence of anticyclonic systems and the likelihood of high-temperature anomalies over Europe. Meanwhile, the weakening of atmospheric circulation could also impact the identified circulation anomalies in section 6b. To some extent, the circulation anomalies related to warmer summer WBT (Fig. 7) can persist longer under decreasing EKE. This persistence may be connected to an increased probability of amplified stationary waves with the weakening circulation, which can further reinforce

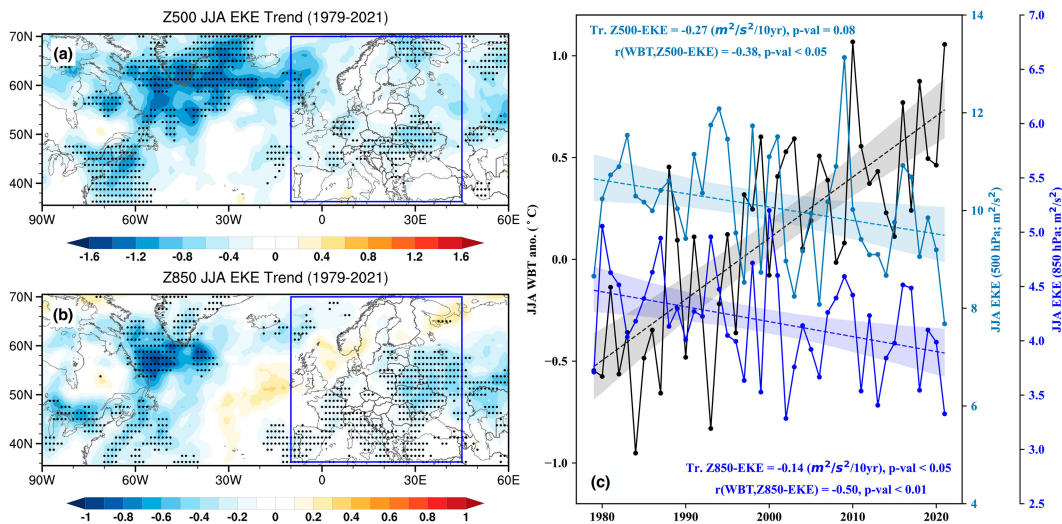


FIG. 11. Trends of summer EKE ($m^2 s^{-2} decade^{-1}$) at (a) 500 and (b) 850 hPa for the period 1979–2021. (c) Time series and linear trends of summer WBT anomalies, EKE at 500 hPa, and EKE at 850 hPa over the European region (blue box). The stippling indicates the trend is significant at the 90% significant level.

warmer summer WBT (Francis and Vavrus 2012; Lin and Yuan 2022).

Last, we employed quantile regression to examine the relationships between summer EKE and WBT anomalies. The analyses are conducted at the 850-hPa level (Fig. 12), with similar results observed in sensitivity analyses at the 500-hPa level (not shown). Spatially, significant negative correlations are found over central and southern Europe, with larger and statistically significant regression slopes observed for the 90th percentile (Fig. 12c), compared to the 10th percentile (Fig. 12a) and the 50th percentile (Fig. 12b). These results indicate that lower EKE values are more strongly associated with higher WBT values, while lower WBT values are related to relatively higher EKE values. This finding is consistent with the study by Lehmann and Coumou (2015), which focused solely on summer temperatures. For the whole European region, we examine EKE values for different quantiles ranging from the 10th percentile to the 90th percentile and compare the results with those obtained from ordinary least squares regression (OLS). As depicted in Figs. 12d and 12e, we highlight the robust and consistent negative relationships observed in all quantile regressions, which corroborate the findings of the OLS regression. These results emphasize the strong and consistent inverse relationship between summer EKE and WBT over Europe.

8. Summary and conclusions

In this study, we aimed to contribute to the understanding of the spatiotemporal variations of summer WBT in Europe and to unravel their potentially underlying driving mechanisms. Elucidating summer WBT variations is crucial, as WBT serves as an effective indicator of heat stress, being strongly influenced by high temperatures and humidity levels, with significant impacts on human health. By employing a variety of datasets and methodologies, we have unveiled a robust and consistent increasing trend of $\sim 1^{\circ}C$ in the summer WBT over central and eastern

Europe from 1958 to 2021. The rate of summer WBT warming in Europe surpasses that of other midlatitude regions, emphasizing an intensified risk of heat stress. Both surface temperature and specific humidity contribute positively to this warming trend, with temperature exerting a slightly greater influence compared to humidity.

We identified four leading modes of European summer WBT after linearly detrending the dataset prior to the analysis. Our investigation highlights the connection between oceanic and atmospheric drivers and the dominant modes of summer WBT at various time scales. At the interdecadal to multidecadal scale, the AMV, DMI, and ENSO, along with corresponding SST anomalies, are associated with the first and second modes of summer WBT. This underscores the crucial role of both local and remote SST anomalies in modulating summer WBT variability, with a preference for long-term time scales (Raymond et al. 2017; Ning et al. 2022). At the interannual time scale, atmospheric internal variability represented by the NAO and AO dominate and influence the third and fourth modes of summer WBT. These results provide valuable insights and support for region-specific seasonal and subseasonal forecasts of summer WBT evolution over Europe.

In addition, we contribute to exploring the impact of global warming and trends in midlatitude circulation on European summer WBT. Besides factors like climate variability, such as the AMV, anthropogenic global warming emerges as a clear signal related to summer WBT variations, consistent with previous studies (Li et al. 2017; Knutson and Ploshay 2016). We acknowledge that recent evidence questions the existence of internal Atlantic multidecadal oscillations in climate systems (Mann et al. 2021). Nevertheless, the interaction between global warming and AMV/AMOC variability can still exert substantial influences on European summer climate (Jackson et al. 2015; Ionita et al. 2022). While observations and climate projections suggest a weakening of AMOC due to greenhouse

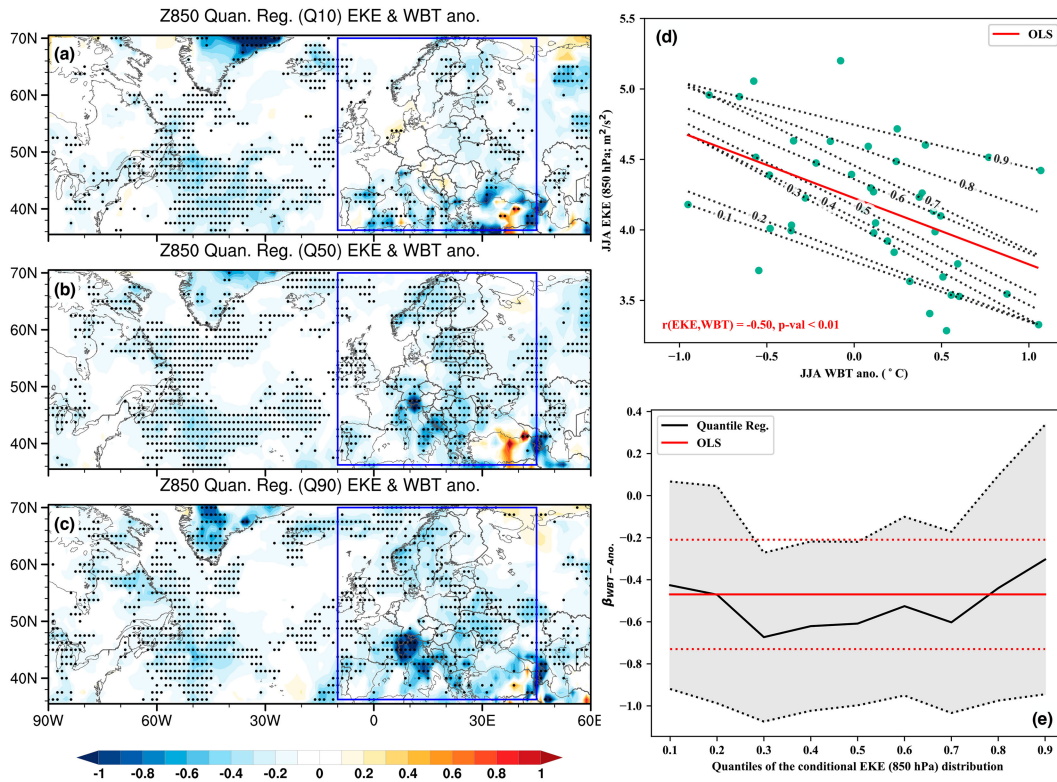


FIG. 12. Quantile regression slopes of the (a) 10th percentile (Q10), (b) 50th percentile (Q50), and (c) 90th percentile (Q90) of EKE (850 hPa) and WBT anomalies in summer (1979–2021). (d) Scatterplot of the European averaged EKE vs WBT anomalies, the quantile regression lines (gray dashed) from the quantile levels 0.1 to 0.9, and the fitted ordinary least squares regression (OLS) line (red solid). (e) Quantile regression coefficients (black curve) and their 90% confidence intervals (gray shading) are compared to the results of the OLS regression (red solid line) and its 90% confidence intervals (red dashed line).

gas emissions (Caesar et al. 2018), leading to a general cooling in the NH through fast climate feedbacks (Jackson et al. 2015; Drijfhout 2015), this cooling may not completely offset the effects of global warming on increasing summer WBT over Europe (Bonnet et al. 2021). Further modeling research is needed, given the limited observation period of AMOC. Moreover, Arctic amplification, another prominent manifestation of global warming, may contribute to midlatitude circulation weakening (Coumou et al. 2015; Screen and Simmonds 2010; Chen and Dai 2022), which, in turn, is associated with warmer summer WBT over Europe.

We have analyzed the possible driving mechanisms separately; however, it is important to note that these driving mechanisms are interconnected across various time scales, involving complex interactions among atmospheric and oceanic circulations and their feedbacks. Our results support the mechanism where anomalous SST warming over the Gulf Stream region triggers a positive phase of a circumglobal wave train, significantly impacting variations in European temperature and precipitation (Saeed et al. 2014). Observations and climate models indicate a rapid warming trend in the western boundary current, including the Gulf Stream (Yang et al. 2016), implying a strengthening of the circumglobal wave train, which could further contribute to increased summer WBT over central and eastern Europe. Further dedicated modeling research would be valuable to quantify the pure

contributions of the atmosphere and ocean and their nonlinear responses to WBT variability. Overall, our findings provide scientific information for decision-makers and policymakers, helping them better understand summer WBT and anticipate the increasing risk of heat stress in Europe in the context of ongoing climate change.

Acknowledgments. We thank Dr. M. Ting for her suggestions that greatly improved the manuscript. This work was supported by funding from the Federal Ministry of Education and Research (BMBF) and the Helmholtz Research Field Earth and Environment for the Innovation Pool Project SCENIC and the Helmholtz Climate Initiative REKLIM. YC was funded by the UK Natural Environment Research Council LTS-S award NE/R016518/1. MI was partially supported by a grant of the Ministry of Research, Innovation and Digitization, under the “Romania’s National Recovery and Resilience Plan - Funded by EU - NextGenerationEU” program, project “Compound extreme events from a long-term perspective and their impact on forest growth dynamics (CEXForD)” number 760074/23.05.2023, code 287/30.11.2022, within Pillar III, Component C9, Investment 8.

Data availability statement. The climate indices are collected from the KNMI Climate Explorer (<https://climexp.knmi.nl/>). We acknowledge the E-OBS dataset and the data providers

in the ECA&D project (<https://www.ecad.eu>) and the data are available from Copernicus Climate Change Service (<https://cds.climate.copernicus.eu/>). The Japanese 55-year Reanalysis data are available from <https://rda.ucar.edu/datasets/ds628.0/>.

REFERENCES

- Barriopedro, D., R. García-Herrera, C. Ordóñez, D. Miralles, and S. Salcedo-Sanz, 2023: Heat waves: Physical understanding and scientific challenges. *Rev. Geophys.*, **61**, e2022RG000780, <https://doi.org/10.1029/2022RG000780>.
- Behera, S., J. V. Ratnam, Y. Masumoto, and T. Yamagata, 2013: Origin of extreme summers in Europe: The Indo-Pacific connection. *Climate Dyn.*, **41**, 663–676, <https://doi.org/10.1007/s00382-012-1524-8>.
- Bekris, Y., P. C. Loikith, and J. D. Neelin, 2023: Short warm distribution tails accelerate the increase of humid-heat extremes under global warming. *Geophys. Res. Lett.*, **50**, e2022GL102164, <https://doi.org/10.1029/2022GL102164>.
- Bladé, I., B. Liebmann, D. Fortuny, and G. J. van Oldenborgh, 2012: Observed and simulated impacts of the summer NAO in Europe: Implications for projected drying in the Mediterranean region. *Climate Dyn.*, **39**, 709–727, <https://doi.org/10.1007/s00382-011-1195-x>.
- Bonnet, R., and Coauthors, 2021: Increased risk of near term global warming due to a recent AMOC weakening. *Nat. Commun.*, **12**, 6108, <https://doi.org/10.1038/s41467-021-26370-0>.
- Brogli, R., S. L. Sørland, N. Kröner, and C. Schär, 2019: Causes of future Mediterranean precipitation decline depend on the season. *Environ. Res. Lett.*, **14**, 114017, <https://doi.org/10.1088/1748-9326/ab4438>.
- , —, —, and —, 2021: Future summer warming pattern under climate change is affected by lapse-rate changes. *Wea. Climate Dyn.*, **2**, 1093–1110, <https://doi.org/10.5194/wcd-2-1093-2021>.
- Buzan, J. R., and M. Huber, 2020: Moist heat stress on a hotter earth. *Annu. Rev. Earth Planet. Sci.*, **48**, 623–655, <https://doi.org/10.1146/annurev-earth-053018-060100>.
- , K. Oleson, and M. Huber, 2015: Implementation and comparison of a suite of heat stress metrics within the Community Land Model version 4.5. *Geosci. Model Dev.*, **8**, 151–170, <https://doi.org/10.5194/gmd-8-151-2015>.
- Byrne, M. P., and P. A. O’Gorman, 2018: Trends in continental temperature and humidity directly linked to ocean warming. *Proc. Natl. Acad. Sci. USA*, **115**, 4863–4868, <https://doi.org/10.1073/pnas.1722312115>.
- Caesar, L., S. Rahmstorf, A. Robinson, G. Feulner, and V. Saba, 2018: Observed fingerprint of a weakening Atlantic Ocean overturning circulation. *Nature*, **556**, 191–196, <https://doi.org/10.1038/s41586-018-0006-5>.
- Cassou, C., L. Terray, and A. S. Phillips, 2005: Tropical Atlantic influence on European heat waves. *J. Climate*, **18**, 2805–2811, <https://doi.org/10.1175/JCLI3506.1>.
- Chen, X., and A. Dai, 2022: Response of meridional wind to greenhouse gas forcing, Arctic sea-ice loss, and Arctic amplification. *J. Climate*, **35**, 7275–7297, <https://doi.org/10.1175/JCLI-D-22-0023.1>.
- Cleveland, W. S., 1979: Robust locally weighted regression and smoothing scatterplots. *J. Amer. Stat. Assoc.*, **74**, 829–836, <https://doi.org/10.1080/01621459.1979.10481038>.
- Coffel, E. D., R. M. Horton, and A. de Sherbinin, 2018: Temperature and humidity based projections of a rapid rise in global heat stress exposure during the 21st century. *Environ. Res. Lett.*, **13**, 014001, <https://doi.org/10.1088/1748-9326/aaa00e>.
- Cohen, J., and M. Barlow, 2005: The NAO, the AO, and global warming: How closely related? *J. Climate*, **18**, 4498–4513, <https://doi.org/10.1175/JCLI3530.1>.
- , and Coauthors, 2014: Recent Arctic amplification and extreme mid-latitude weather. *Nat. Geosci.*, **7**, 627–637, <https://doi.org/10.1038/ngeo2234>.
- Cornes, R. C., G. van der Schrier, E. J. van den Besselaar, and P. D. Jones, 2018: An ensemble version of the E-OBS temperature and precipitation data sets. *J. Geophys. Res. Atmos.*, **123**, 9391–9409, <https://doi.org/10.1029/2017JD028200>.
- Coumou, D., J. Lehmann, and J. Beckmann, 2015: The weakening summer circulation in the Northern Hemisphere mid-latitudes. *Science*, **348**, 324–327, <https://doi.org/10.1126/science.1261768>.
- , G. Di Capua, S. Vavrus, L. Wang, and S. Wang, 2018: The influence of Arctic amplification on mid-latitude summer circulation. *Nat. Commun.*, **9**, 2959, <https://doi.org/10.1038/s41467-018-05256-8>.
- Davies-Jones, R., 2008: An efficient and accurate method for computing the wet-bulb temperature along pseudoadiabats. *Mon. Wea. Rev.*, **136**, 2764–2785, <https://doi.org/10.1175/2007MWR2224.1>.
- Davis, R. E., G. R. McGregor, and K. B. Enfield, 2016: Humidity: A review and primer on atmospheric moisture and human health. *Environ. Res.*, **144**, 106–116, <https://doi.org/10.1016/j.envres.2015.10.014>.
- Della-Marta, P. M., J. Luterbacher, H. von Weissenfluh, E. Xoplaki, M. Brunet, and H. Wanner, 2007: Summer heat waves over Western Europe 1880–2003, their relationship to large-scale forcings and predictability. *Climate Dyn.*, **29**, 251–275, <https://doi.org/10.1007/s00382-007-0233-1>.
- DelSole, T., M. K. Tippett, and J. Shukla, 2011: A significant component of unforced multidecadal variability in the recent acceleration of global warming. *J. Climate*, **24**, 909–926, <https://doi.org/10.1175/2010JCLI3659.1>.
- Diffenbaugh, N. S., J. S. Pal, F. Giorgi, and X. Gao, 2007: Heat stress intensification in the Mediterranean climate change hotspot. *Geophys. Res. Lett.*, **34**, L11706, <https://doi.org/10.1029/2007GL030000>.
- Dima, M., and G. Lohmann, 2007: A hemispheric mechanism for the Atlantic multidecadal oscillation. *J. Climate*, **20**, 2706–2719, <https://doi.org/10.1175/JCLI4174.1>.
- Dong, B., R. T. Sutton, T. Woollings, and K. Hodges, 2013: Variability of the North Atlantic summer storm track: Mechanisms and impacts on European climate. *Environ. Res. Lett.*, **8**, 034037, <https://doi.org/10.1088/1748-9326/8/3/034037>.
- , —, and L. Shaffrey, 2017: Understanding the rapid summer warming and changes in temperature extremes since the mid-1990s over western Europe. *Climate Dyn.*, **48**, 1537–1554, <https://doi.org/10.1007/s00382-016-3158-8>.
- Drijfhout, S., 2015: Competition between global warming and an abrupt collapse of the AMOC in Earth’s energy imbalance. *Sci. Rep.*, **5**, 14877, <https://doi.org/10.1038/srep14877>.
- England, M. R., I. Eisenman, N. J. Lutsko, and T. J. Wagner, 2021: The recent emergence of Arctic amplification. *Geophys. Res. Lett.*, **48**, e2021GL094086, <https://doi.org/10.1029/2021GL094086>.
- Ferranti, L., S. Corti, and M. Janousek, 2015: Flow-dependent verification of the ECMWF ensemble over the Euro-Atlantic sector. *Quart. J. Roy. Meteor. Soc.*, **141**, 916–924, <https://doi.org/10.1002/qj.2411>.
- Fischer, E. M., and R. Knutti, 2013: Robust projections of combined humidity and temperature extremes. *Nat. Climate Change*, **3**, 126–130, <https://doi.org/10.1038/nclimate1682>.

- , S. I. Seneviratne, D. Lüthi, and C. Schär, 2007: Contribution of land-atmosphere coupling to recent European summer heat waves. *Geophys. Res. Lett.*, **34**, L06707, <https://doi.org/10.1029/2006GL029068>.
- Folland, C. K., J. Knight, H. W. Linderholm, D. Fereday, S. Ineson, and J. W. Hurrell, 2009: The summer North Atlantic Oscillation: Past, present, and future. *J. Climate*, **22**, 1082–1103, <https://doi.org/10.1175/2008JCLI2459.1>.
- Francis, J. A., and S. J. Vavrus, 2012: Evidence linking Arctic amplification to extreme weather in mid-latitudes. *Geophys. Res. Lett.*, **39**, L06801, <https://doi.org/10.1029/2012GL051000>.
- Gao, M., and C. L. Franzke, 2017: Quantile regression-based spatio-temporal analysis of extreme temperature change in China. *J. Climate*, **30**, 9897–9914, <https://doi.org/10.1175/JCLI-D-17-0356.1>.
- Ghosh, R., W. A. Müller, J. Baehr, and J. Bader, 2017: Impact of observed North Atlantic multidecadal variations to European summer climate: A linear baroclinic response to surface heating. *Climate Dyn.*, **48**, 3547–3563, <https://doi.org/10.1007/s00382-016-3283-4>.
- Hirschi, M., and Coauthors, 2011: Observational evidence for soil-moisture impact on hot extremes in southeastern Europe. *Nat. Geosci.*, **4**, 17–21, <https://doi.org/10.1038/ngeo1032>.
- Hochman, A., G. Messori, J. F. Quinting, J. G. Pinto, and C. M. Grams, 2021: Do Atlantic-European weather regimes physically exist? *Geophys. Res. Lett.*, **48**, e2021GL095574, <https://doi.org/10.1029/2021GL095574>.
- Horton, D. E., N. C. Johnson, D. Singh, D. L. Swain, B. Rajaratnam, and N. S. Diffenbaugh, 2015: Contribution of changes in atmospheric circulation patterns to extreme temperature trends. *Nature*, **522**, 465–469, <https://doi.org/10.1038/nature14550>.
- Horton, R. M., J. S. Mankin, C. Lesk, E. Coffel, and C. Raymond, 2016: A review of recent advances in research on extreme heat events. *Curr. Climate Change Rep.*, **2**, 242–259, <https://doi.org/10.1007/s40641-016-0042-x>.
- Hu, S., and A. V. Fedorov, 2019: Indian Ocean warming can strengthen the Atlantic meridional overturning circulation. *Nat. Climate Change*, **9**, 747–751, <https://doi.org/10.1038/s41558-019-0566-x>.
- Huang, B., and Coauthors, 2017: Extended Reconstructed Sea Surface Temperature, version 5 (ERSSTv5): Upgrades, validations, and intercomparisons. *J. Climate*, **30**, 8179–8205, <https://doi.org/10.1175/JCLI-D-16-0836.1>.
- Ionita, M., N. Rimbu, S. Chelcea, and S. Patrut, 2013: Multidecadal variability of summer temperature over Romania and its relation with Atlantic multidecadal oscillation. *Theor. Appl. Climatol.*, **113**, 305–315, <https://doi.org/10.1007/s00704-012-0786-8>.
- , C. Boronean, and S. Chelcea, 2015: Seasonal modes of dryness and wetness variability over Europe and their connections with large scale atmospheric circulation and global sea surface temperature. *Climate Dyn.*, **45**, 2803–2829, <https://doi.org/10.1007/s00382-015-2508-2>.
- , and Coauthors, 2017: The European 2015 drought from a climatological perspective. *Hydrol. Earth Syst. Sci.*, **21**, 1397–1419, <https://doi.org/10.5194/hess-21-1397-2017>.
- , V. Nagavciuc, R. Kumar, and O. Rakovec, 2020: On the curious case of the recent decade, mid-spring precipitation deficit in Central Europe. *npj Climate Atmos. Sci.*, **3**, 49, <https://doi.org/10.1038/s41612-020-00153-8>.
- , D. E. Caldarescu, and V. Nagavciuc, 2021: Compound hot and dry events in Europe: Variability and large-scale drivers. *Front. Climate*, **3**, 688991, <https://doi.org/10.3389/fclim.2021.688991>.
- , V. Nagavciuc, P. Scholz, and M. Dima, 2022: Long-term drought intensification over Europe driven by the weakening trend of the Atlantic meridional overturning circulation. *J. Hydrol.*, **42**, 101176, <https://doi.org/10.1016/j.ejrh.2022.101176>.
- Jackson, L., R. Kahana, T. Graham, M. Ringer, T. Woollings, J. Mecking, and R. Wood, 2015: Global and European climate impacts of a slowdown of the AMOC in a high resolution GCM. *Climate Dyn.*, **45**, 3299–3316, <https://doi.org/10.1007/s00382-015-2540-2>.
- Knutson, T. R., and J. J. Ploshay, 2016: Detection of anthropogenic influence on a summertime heat stress index. *Climatic Change*, **138**, 25–39, <https://doi.org/10.1007/s10584-016-1708-z>.
- Kobayashi, S., and Coauthors, 2015: The JRA-55 reanalysis: General specifications and basic characteristics. *J. Meteor. Soc. Japan*, **93**, 5–48, <https://doi.org/10.2151/jmsj.2015-001>.
- Kodra, E., and A. R. Ganguly, 2014: Asymmetry of projected increases in extreme temperature distributions. *Sci. Rep.*, **4**, 5884, <https://doi.org/10.1038/srep05884>.
- Koenker, R., and G. Bassett Jr., 1978: Regression quantiles. *Econometrica*, **46**, 33–50, <https://doi.org/10.2307/1913643>.
- Kornhuber, K., S. Osprey, D. Coumou, S. Petri, V. Petoukhov, S. Rahmstorf, and L. Gray, 2019: Extreme weather events in early summer 2018 connected by a recurrent hemispheric wave-7 pattern. *Environ. Res. Lett.*, **14**, 054002, <https://doi.org/10.1088/1748-9326/ab13bf>.
- Latif, M., J. Sun, M. Visbeck, and M. Hadi Bordbar, 2022: Natural variability has dominated Atlantic meridional overturning circulation since 1900. *Nat. Climate Change*, **12**, 455–460, <https://doi.org/10.1038/s41558-022-01342-4>.
- Lehmann, J., and D. Coumou, 2015: The influence of mid-latitude storm tracks on hot, cold, dry and wet extremes. *Sci. Rep.*, **5**, 17491, <https://doi.org/10.1038/srep17491>.
- , —, K. Frieler, A. V. Eliseev, and A. Levermann, 2014: Future changes in extratropical storm tracks and baroclinicity under climate change. *Environ. Res. Lett.*, **9**, 084002, <https://doi.org/10.1088/1748-9326/9/8/084002>.
- Li, C., X. Zhang, F. Zwiers, Y. Fang, and A. M. Michalak, 2017: Recent very hot summers in Northern Hemispheric land areas measured by wet bulb globe temperature will be the norm within 20 years. *Earth's Future*, **5**, 1203–1216, <https://doi.org/10.1002/2017EF000639>.
- Li, J., Y. D. Chen, T. Y. Gan, and N.-C. Lau, 2018: Elevated increases in human-perceived temperature under climate warming. *Nat. Climate Change*, **8**, 43–47, <https://doi.org/10.1038/s41558-017-0036-2>.
- Li, M., Y. Yao, I. Simmonds, D. Luo, L. Zhong, and X. Chen, 2020: Collaborative impact of the NAO and atmospheric blocking on European heatwaves, with a focus on the hot summer of 2018. *Environ. Res. Lett.*, **15**, 114003, <https://doi.org/10.1088/1748-9326/aba6ad>.
- Lin, Q., and J. Yuan, 2022: Linkages between amplified quasi-stationary waves and humid heat extremes in Northern Hemisphere midlatitudes. *J. Climate*, **35**, 8245–8258, <https://doi.org/10.1175/JCLI-D-21-0952.1>.
- Liu, Y., M. Garcia, C. Zhang, and Q. Tang, 2022: Recent decrease in summer precipitation over the Iberian Peninsula closely links to reduction in local moisture recycling. *Hydrol. Earth Syst. Sci.*, **26**, 1925–1936, <https://doi.org/10.5194/hess-26-1925-2022>.
- Ma, Q., and C. L. E. Franzke, 2021: The role of transient eddies and diabatic heating in the maintenance of European heat waves: A nonlinear quasi-stationary wave perspective. *Climate Dyn.*, **56**, 2983–3002, <https://doi.org/10.1007/s00382-021-05628-9>.

- , V. Lembo, and C. L. E. Franzke, 2021: The Lorenz energy cycle: Trends and the impact of modes of climate variability. *Tellus*, **73A**, 1900033, <https://doi.org/10.1080/16000870.2021.1900033>.
- Mann, M. E., B. A. Steinman, D. J. Brouillette, and S. K. Miller, 2021: Multidecadal climate oscillations during the past millennium driven by volcanic forcing. *Science*, **371**, 1014–1019, <https://doi.org/10.1126/science.abc5810>.
- Martija-Díez, M., B. Rodríguez-Fonseca, and J. López-Parages, 2021: ENSO influence on western European summer and fall temperatures. *J. Climate*, **34**, 8013–8031, <https://doi.org/10.1175/JCLI-D-20-0808.1>.
- Matthews, T., M. Byrne, R. Horton, C. Murphy, R. Pielke Sr., C. Raymond, P. Thorne, and R. L. Wilby, 2022: Latent heat must be visible in climate communications. *Wiley Interdiscip. Rev.: Climate Change*, **13**, e779, <https://doi.org/10.1002/wcc.779>.
- Ning, G., M. Luo, S. Wang, Z. Liu, P. Wang, and Y. Yang, 2022: Dominant modes of summer wet bulb temperature in China. *Climate Dyn.*, **59**, 1473–1488, <https://doi.org/10.1007/s00382-021-06051-w>.
- North, G. R., T. L. Bell, R. F. Cahalan, and F. J. Moeng, 1982: Sampling errors in the estimation of empirical orthogonal functions. *Mon. Wea. Rev.*, **110**, 699–706, [https://doi.org/10.1175/1520-0493\(1982\)110<0699:SEITEO>2.0.CO;2](https://doi.org/10.1175/1520-0493(1982)110<0699:SEITEO>2.0.CO;2).
- Pedersen, R. A., I. Cvijanovic, P. L. Langen, and B. M. Vinther, 2016: The impact of regional Arctic sea ice loss on atmospheric circulation and the NAO. *J. Climate*, **29**, 889–902, <https://doi.org/10.1175/JCLI-D-15-0315.1>.
- Peel, M. C., B. L. Finlayson, and T. A. McMahon, 2007: Updated world map of the Köppen-Geiger climate classification. *Hydro. Earth Syst. Sci.*, **11**, 1633–1644, <https://doi.org/10.5194/hess-11-1633-2007>.
- Raymond, C., D. Singh, and R. Horton, 2017: Spatiotemporal patterns and synoptics of extreme wet-bulb temperature in the contiguous United States. *J. Geophys. Res. Atmos.*, **122**, 13 108–13 124, <https://doi.org/10.1002/2017JD027140>.
- , T. Matthews, and R. M. Horton, 2020: The emergence of heat and humidity too severe for human tolerance. *Sci. Adv.*, **6**, eaaw1838, <https://doi.org/10.1126/sciadv.aaw1838>.
- Rhines, A., K. A. McKinnon, M. P. Tingley, and P. Huybers, 2017: Seasonally resolved distributional trends of North American temperatures show contraction of winter variability. *J. Climate*, **30**, 1139–1157, <https://doi.org/10.1175/JCLI-D-16-0363.1>.
- Rogers, C. D., M. Ting, C. Li, K. Kornhuber, E. D. Coffel, R. M. Horton, C. Raymond, and D. Singh, 2021: Recent increases in exposure to extreme humid-heat events disproportionately affect populated regions. *Geophys. Res. Lett.*, **48**, e2021GL094183, <https://doi.org/10.1029/2021GL094183>.
- Rousi, E., K. Kornhuber, G. Beobide-Arsuaga, F. Luo, and D. Coumou, 2022: Accelerated western European heatwave trends linked to more-persistent double jets over Eurasia. *Nat. Commun.*, **13**, 3851, <https://doi.org/10.1038/s41467-022-31432-y>.
- Russo, S., and Coauthors, 2014: Magnitude of extreme heat waves in present climate and their projection in a warming world. *J. Geophys. Res. Atmos.*, **119**, 12 500–12 512, <https://doi.org/10.1002/2014JD022098>.
- , J. Sillmann, and A. Sterl, 2017: Humid heat waves at different warming levels. *Sci. Rep.*, **7**, 7477, <https://doi.org/10.1038/s41598-017-07536-7>.
- Saeed, S., N. V. Lipzig, W. A. Müller, F. Saeed, and D. Zanchettin, 2014: Influence of the circumglobal wave-train on European summer precipitation. *Climate Dyn.*, **43**, 503–515, <https://doi.org/10.1007/s00382-013-1871-0>.
- Screen, J. A., and I. Simmonds, 2010: The central role of diminishing sea ice in recent Arctic temperature amplification. *Nature*, **464**, 1334–1337, <https://doi.org/10.1038/nature09051>.
- Sherwood, S. C., and M. Huber, 2010: An adaptability limit to climate change due to heat stress. *Proc. Natl. Acad. Sci. USA*, **107**, 9552–9555, <https://doi.org/10.1073/pnas.0913352107>.
- Smith, S. J., J. van Aardenne, Z. Klimont, R. J. Andres, A. Volke, and S. Delgado Arias, 2011: Anthropogenic sulfur dioxide emissions: 1850–2005. *Atmos. Chem. Phys.*, **11**, 1101–1116, <https://doi.org/10.5194/acp-11-1101-2011>.
- Stull, R., 2011: Wet-bulb temperature from relative humidity and air temperature. *J. Appl. Meteor. Climatol.*, **50**, 2267–2269, <https://doi.org/10.1175/JAMC-D-11-0143.1>.
- Sutton, R. T., and D. L. Hodson, 2005: Atlantic Ocean forcing of North American and European summer climate. *Science*, **309**, 115–118, <https://doi.org/10.1126/science.1109496>.
- , and B. Dong, 2012: Atlantic Ocean influence on a shift in European climate in the 1990s. *Nat. Geosci.*, **5**, 788–792, <https://doi.org/10.1038/ngeo1595>.
- Teng, H., R. Leung, G. Branstator, J. Lu, and Q. Ding, 2022: Warming pattern over the Northern Hemisphere midlatitudes in boreal summer 1979–2020. *J. Climate*, **35**, 3479–3494, <https://doi.org/10.1175/JCLI-D-21-0437.1>.
- Thompson, D. W. J., and J. M. Wallace, 1998: The Arctic oscillation signature in the wintertime geopotential height and temperature fields. *Geophys. Res. Lett.*, **25**, 1297–1300, <https://doi.org/10.1029/98GL00950>.
- , and —, 2001: Regional climate impacts of the Northern Hemisphere Annular Mode. *Science*, **293**, 85–89, <https://doi.org/10.1126/science.1058958>.
- Tuel, A., and E. A. Eltahir, 2021: Mechanisms of European summer drying under climate change. *J. Climate*, **34**, 8913–8931, <https://doi.org/10.1175/JCLI-D-20-0968.1>.
- Vihma, T., 2014: Effects of Arctic sea ice decline on weather and climate: A review. *Surv. Geophys.*, **35**, 1175–1214, <https://doi.org/10.1007/s10712-014-9284-0>.
- Wang, P., L. R. Leung, J. Lu, F. Song, and J. Tang, 2019: Extreme wet-bulb temperatures in China: The significant role of moisture. *J. Geophys. Res. Atmos.*, **124**, 11 944–11 960, <https://doi.org/10.1029/2019JD031477>.
- , Y. Yang, J. Tang, L. R. Leung, and H. Liao, 2021: Intensified humid heat events under global warming. *Geophys. Res. Lett.*, **48**, e2020GL091462, <https://doi.org/10.1029/2020GL091462>.
- Wilks, D., 2016: “The stippling shows statistically significant grid points”: How research results are routinely overstated and overinterpreted, and what to do about it. *Bull. Amer. Meteor. Soc.*, **97**, 2263–2273, <https://doi.org/10.1175/BAMS-D-15-00267.1>.
- Yang, H., G. Lohmann, W. Wei, M. Dima, M. Ionita, and J. Liu, 2016: Intensification and poleward shift of subtropical western boundary currents in a warming climate. *J. Geophys. Res. Oceans*, **121**, 4928–4945, <https://doi.org/10.1002/2015JC011513>.
- Yu, S., S. F. B. Tett, N. Freychet, and Z. Yan, 2021: Changes in regional wet heatwave in Eurasia during summer (1979–2017). *Environ. Res. Lett.*, **16**, 064094, <https://doi.org/10.1088/1748-9326/ac0745>.
- Yue, S., and C. Y. Wang, 2002: Applicability of prewhitening to eliminate the influence of serial correlation on the Mann-

- Kendall test. *Water Resour. Res.*, **38**, 1068, <https://doi.org/10.1029/2001WR000861>.
- Zhang, R., C. Sun, J. Zhu, R. Zhang, and W. Li, 2020: Increased European heat waves in recent decades in response to shrinking Arctic sea ice and Eurasian snow cover. *npj Climate Atmos. Sci.*, **3**, 7, <https://doi.org/10.1038/s41612-020-0110-8>.
- Zhao, L., and Coauthors, 2021: Global multi-model projections of local urban climates. *Nat. Climate Change*, **11**, 152–157, <https://doi.org/10.1038/s41558-020-00958-8>.
- Zschenderlein, P., A. H. Fink, S. Pfahl, and H. Wernli, 2019: Processes determining heat waves across different European climates. *Quart. J. Roy. Meteor. Soc.*, **145**, 2973–2989, <https://doi.org/10.1002/qj.3599>.